Fall 1995

Investigation of potential oxygen defect mechanism of persistent photoconductivity and photoinduced superconductivity in YBa2Cu3Ox

Denise Catherine Chew
New Jersey Institute of Technology

Copyright Warning & Restrictions

The copyright law of the United States (Title 17, United States Code) governs the making of photocopies or other reproductions of copyrighted material.

Under certain conditions specified in the law, libraries and archives are authorized to furnish a photocopy or other reproduction. One of these specified conditions is that the photocopy or reproduction is not to be "used for any purpose other than private study, scholarship, or research." If a, user makes a request for, or later uses, a photocopy or reproduction for purposes in excess of "fair use" that user may be liable for copyright infringement,

This institution reserves the right to refuse to accept a copying order if, in its judgment, fulfillment of the order would involve violation of copyright law.

Please Note: The author retains the copyright while the New Jersey Institute of Technology reserves the right to distribute this thesis or dissertation

Printing note: If you do not wish to print this page, then select "Pages from: first page # to: last page #" on the print dialog screen

ABSTRACT

INVESTIGATION OF POTENTIAL OXYGEN DEFECT MECHANISM OF PERSISTENT PHOTOCONDUCTIVITY AND PHOTOINDUCED SUPERCONDUCTIVITY IN $YBa_2Cu_3O_x$

by
Denise Catherine Chew

In this thesis work, we conclude that oxygen vacancy defects play a fundamental role in the PPC/PISC mechanism and identify the oxygen defects as F centers (an oxygen vacancy which traps two electrons) or F^+ centers. Also, the correlation between the peaks observed in the luminescence spectra and those observed in the wavelength dependence of PPC suggest that the photogeneration of charges and their annihilation via luminescent recombination occur in the same level (Cu-O chains) of the $YBa_2Cu_3O_x$ crystal. Previous models had assigned the peaks in the PPC excitation spectrum to charge transfer in the CuO_2 planes. In addition, photoluminescence and infrared spectroscopy are used to characterize the energy levels of the defects.

INVESTIGATION OF POTENTIAL OXYGEN DEFECT MECHANISM OF PERSISTENT PHOTOCONDUCTIVITY AND PHOTOINDUCED SUPERCONDUCTIVITY IN $YBa_2Cu_3O_x$

by
Denise Catherine Chew

A Thesis
Submitted to the Faculty of
New Jersey Institute of Technology
in Partial Fulfillment of the Requirements for the Degree of
Master of Science in Applied Physics

Department of Physics

January 1996

APPROVAL PAGE

INVESTIGATION OF POTENTIAL OXYGEN DEFECT MECHANISM OF PERSISTENT PHOTOCONDUCTIVITY AND PHOTOINDUCED SUPERCONDUCTIVITY IN $YBa_2Cu_3O_x$

Denise Catherine Chew

Dr. John Federici, Thesis Advisor — Date
Assistant Professor of Physics
New Jersey Institute of Technology

Dr. William Savin, Committee Member — Date
Professor of Physics
New Jersey Institute of Technology

Dr. William Wilber, Committee Member — Date
HTSC Group Leader, Physical Science Directorate
Army Research Laboratory

BIOGRAPHICAL SKETCH

Author: Denise Catherine Chew

Degree: Master of Science

Undergraduate and Graduate Education:

- Master of Science in Applied Physics,
  New Jersey Institute of Technology, Newark, NJ, 1996

- Bachelor of Science in Physics,
  Eastern Nazarene College, Quincy, MA, 1994

Major: Applied Physics

Presentations and Publications:

D. C. Chew, J. F. Federici, W. Savin, and W. Wilber,
Defect Mechanism of Photoinduced Superconductivity in YBCO,
Proceedings of the 1995 Fall meeting of the Materials Research Society,
Boston, USA, 193,(1995).

J. F. Federici, D. Chew, B. Welker, W. Savin, J. Gutierrez-Solana, T. Fink and W. Wilber, *Phys. Rev. B*, **52**, 52, (1995).

To Those Who have Taught:

He who knows not, and knows not that he knows not, is a fool - shun him. He who knows not, and knows that he knows not, is a child - teach him. He who knows, and knows not that he knows, is wise - follow him.

PERSIAN PROVERB

ACKNOWLEDGMENT

I would like to express my appreciation to Dr. John Federici, of NJIT and Dr. William Wilber of the Army Research Laboratory for their valuable insight, resources and support. I also wish to extend my thanks to Dr. William Savin, Dr. Tobin Fink, Dr. Steven Tidrow, Dr. Arthur Tauber, Dr. Ernest Potenziani, Robert Finnegan, Drew Brocking, Jose Gutierrez-Solana, and Gerry Molina for their assistance. My thanks also to the National Science Foundation whose largesse made the project possible.

TABLE OF CONTENTS

TABLE OF CONTENTS
(Continued)

Chapter Page

LIST OF TABLES

LIST OF FIGURES

LIST OF FIGURES
(Continued)

CHAPTER 1

SUPERCONDUCTIVITY AND $YBa_2Cu_3O_x$

1.1 Superconductivity

Superconductivity [1, 2, 3, 4] occurs because the superconducting state has a lower energy than the normal state of a material. In 1956, physicist Leon Cooper provided a description of a mechanism [5] in which results in a lower energy bound-electron state. An addition of two electrons, whose energy is higher than that of the Fermi energy, to a metal's 'Fermi sea' of free electrons, would essentially increase the total energy of the electron population. However, when two electrons bind together, as if they were a molecular atom, the total energy of the system would be lowered. According to classical physics, any two particles with any degree of attraction can form a bound state with energy lower than that of the two while separate. However, this attractive binding energy between the two particles must be great enough to overcome the kinetic energy of the particles and the inherent Coulombic repulsion of the electrons, which would keep the 'pair' from forming. Cooper was able to show that in the presence of an attractive interaction, two electrons added to the 'Fermi sea' will form a bound pair. Although the pair binding energy is on the order of one-thousandths of the electron energy [4] the proper conditions will enable the pairs to continually recombine in order to maintain a state of lowered energy. On the average, the electrons will spend more time in the paired state than alone, thus lowering the energy of the system.

The lattice itself is also important to the superconducting mechanism. Given that

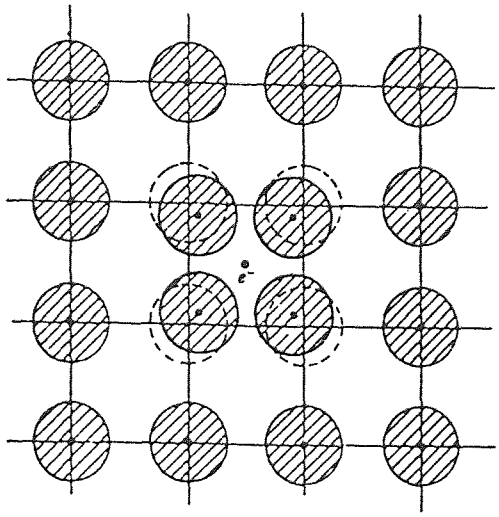

Figure 1.1 : Electron shielding by lattice distortion allowing electron-electron attraction: The formation of Cooper pairs.

Cooper stated that electrons will form a lower energy bound state when provided with an attractive force, it becomes a matter of determining the nature and origin of an unlikely attractive force between two like particles, which by nature repel each other (Coulomb's Law). In 1950, German physicist Herbert Frolich suggested an 'electron-phonon' interaction. It was not until several years later, after Cooper's 1956 proposition, that the mechanism was detailed [5]. An electron attracts nearby ions of opposite charge and distorts the orderly arrangement of the lattice. This distortion effectively 'tugs' on the lattice (modeled as atoms connected by springs) and creates phonons (defined as quantized lattice vibrations). Other electrons then encounter these distortions in the lattice which is now polarized due to the shielding of the first electron by the positive ions. This is illustrated in Figure 1.1. The second electron is attracted by the concentration of positive charge and effectively 'pairs' with the first electron. These lattice distortions are short-lived phenomena, which exist to allow

the electron-electron interactions known as Cooper pairs.

Once the attraction and pairing have been explained for a single electron-electron system, it becomes necessary to consider large numbers of interactions at once. Due to the daunting nature of the theoretical analysis of many-body systems, physicists Bardeen, Cooper, and Schrieffer (BCS) made an assumption. They assumed that only pair interactions are important, thus relegating the role of other electrons to providing constraints on the states to which the interacting pair can scatter (because the electrons must still obey the Pauli Exclusion Principle). This is known as the mean field theory. By using this theory and treating all the electrons in a metal at once, BCS theory [5] was able to provide a mechanism by which one pair lowered the energy, while multiple pairs lowered it even further. First, electrons are scattered through interactions with phonons to a vacant state above the Fermi level, then allowed to interact and form Cooper pairs. Consequently, we have a new state comprised of Cooper pairs. As the number of paired electrons increases, the number of available states to scatter into decreases and thus the number of possible scattering processes decreases. By this means, a point is reached where the amount of energy expended to scatter the electrons to a state where they can pair is greater than the energy decrease provided by the pairing. Eventually, an optimum number of Cooper pairs are formed. Pairs are continually formed and broken preserving this optimum number. An important property of this BCS ground state is that the pairs are completely interchangeable and indistinguishable from one another: All pairs can be described by a single wave function. As bosons, they do not obey Pauli exclusion.

The superconducting state is characterized by three important parameters: 1)tran-

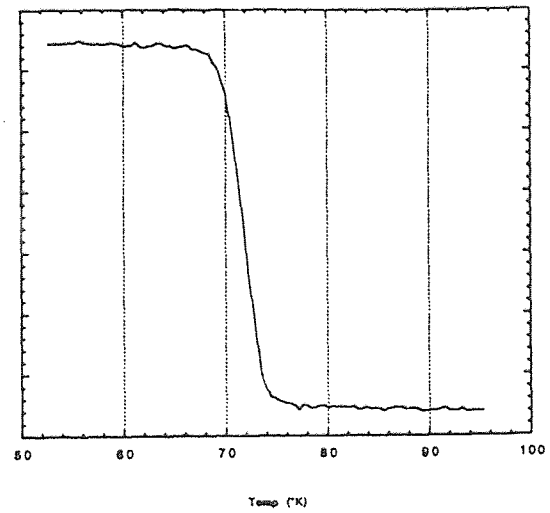

Figure 1.2 : Typical resistance versus temperature curve showing abrupt phase change from normal state to superconducting state.

sition temperature, 2) enhanced conductivity, and 3) diamagnetism. The transition temperature is also referred to as the critical temperature (T_c) and is the point at which the material undergoes a phase transition from the normal state to the superconducting state. As can be seen in Figure 1.2, the phase change at T_c is physically evidenced by an abrupt drop in resistance to zero where consequently conductance peaks to infinity. In comparison, the resistance of a normal metal behaves linearly with temperature. In the early 1930's the superconducting state's perfect diamagnetism was demonstrated by Meissner and is known as the Meissner Effect. BCS theory [5] has been successful in predicting the behavior of low T_c materials such as lead.

1.2 Class I and Class II Materials

However, there are many materials that will superconduct at the proper temperatures which do not fall within the explanation offered by this theory. These mate-

rials, known as Class II superconductors (high T_c materials) are characterized by a deviation in their behavior with respect to the Meissner effect. In a Class I superconductor (low T_c) the magnetic behavior is predicted and accurately modeled on the basis of infinite conductivity. This model assumes that the entire magnetic field can be excluded from the sample. However, in filaments of the sample (size on the order λ) there is penetration of the magnetic field. When these filaments are stabilized by interactions with impurities, dislocations, etc. the superconducting state can persist to much higher temperatures than calculated by the thermodynamic arguments used to predict the behavior of the Class I materials. An inhomogeneous phase is formed and the magnetic flux is transported by these filaments of normal metal interspersed within superconducting material. This intermediate state [2] would seem to be thermodynamically stable and on a macroscopic scale, still electrically superconductive.

Class II superconductors are more likely than Class I Superconductors to result electronic and other applications due to the lower cost to bring these materials to their superconducting state. For many of these materials, liquid nitrogen ($77^{\circ}K$) is sufficient to induce the phase change where as liquid helium ($4^{\circ}K$) is needed for low temperature materials. Currently, the one of the highest temperature superconductoring materials is a mercury based system with a transition temperature of approximately $124^{\circ}K$ [6] which under pressure escalates slightly. A recent paper by a Russian group [7] extols a new Selenium compound reported to have a critical temperature of $390^{\circ}K$. If this is substantiated, it will revolutionize the current applications of superconductors and create many new low cost uses. To date, their data has not yet been duplicated by another group. However, if the data is substantiated,

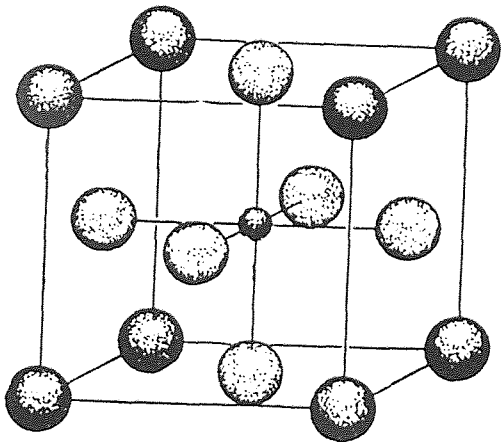

Figure 1.3 : General perovskite structure

it is worth noting that at room temperature ($300^{\circ}K$) a sample would "float" above a magnet due to magnetic flux repulsion.

1.3 $YBa_2Cu_3O_x$

One family of materials known as 1-2-3 materials (from their stoichiometric formulae) has been under much investigation due to relatively high T_c's ($90^{\circ}K$). From this point forward, discussion will center around a particular 1-2-3 compound: $YBa_2Cu_3O_x$. The lattice structure of the $YBa_2Cu_3O_x$ compound is known as an oxygen depleted layered perovskite crystal. The unit cell has a rectangular shape but no two dimensions are the same size. It is also important to note the material is anisotropic; its properties differ according to orientation within the lattice. Perovskite structures of the general formula ABO_3, where A and B are metal ions, are essentially characterized by the tetrahedral distribution of large cations around a center smaller cation and oxygen ions in the centers of the faces. The most general structure (Figure 1.3) can

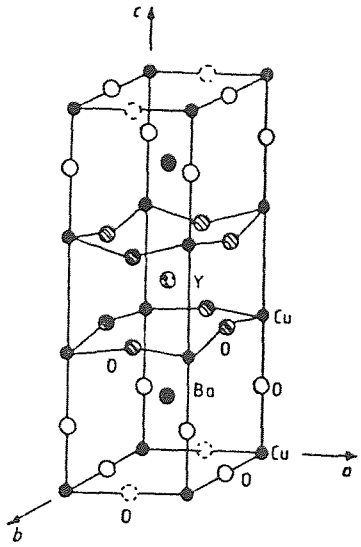

Figure 1.4 : Distorted perovskite structure of $YBa_2Cu_3O_x$

be extended to the $YBa_2Cu_3O_x$ case in which the Cu-O bonds form alternating planes between YBa planes (Figure 1.4). In the case of $YBa_2Cu_3O_x$ properties are generally attributed to the interactions of the oxygen and copper atoms. Alterations in these interactions produce changes in physical parameters and changes in electrical properties.

Oxygen deficiencies are easily produced and lead to nonstoichiometric structure and alterations of the interactions between the copper and oxygen atoms. The removal of oxygen atoms from the lattice has a number of effects. As seen in Figure 1.5, the cell parameters are a function of the x parameter (relative number of oxygen atoms in the lattice). At a particular point, the cell changes from an orthorhombic to tetragonal phase in the vicinity of x=6.5, which does not necessarily correspond to the step in lattice parameter seen in the figure for Zr gettered samples. Cava notes that the orthorhombicty is not a linear function of stoichiometry that would extrapolate to zero at x=6.0 if there were no orthorhombic-tetragonal phase transition. This is due

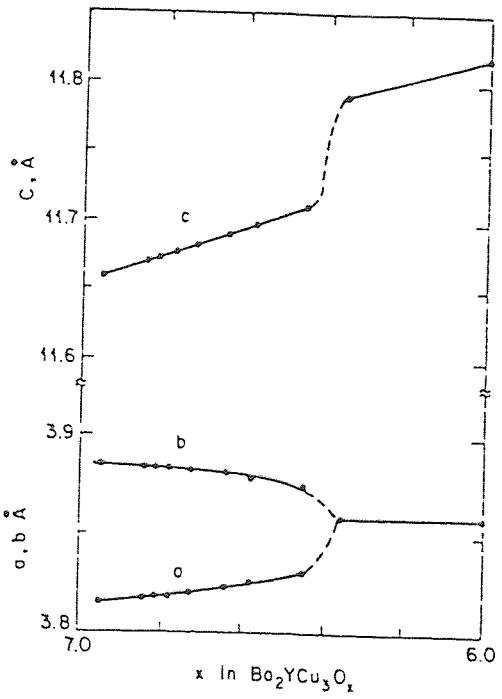

Figure 1.5 : Lattice structure changes as it is deprived of oxygen ions

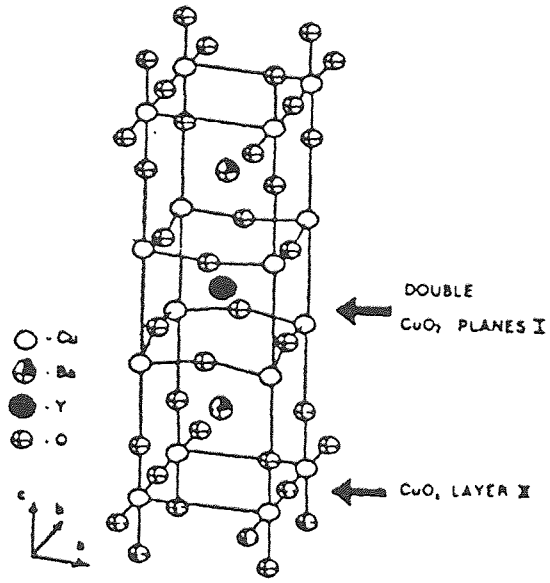

Figure 1.6 : "Chains" and "Layers" in the $YBa_2Cu_3O_x$ structure

to the cooperative phenomena which tends to maintain the integrity of the chains as oxygen is removed. It has been previously shown that the variation in orthorhombicity with oxygen content depends on the annealing temperature [8].

Another effect of increasing oxygen depletion is to change the electrical characteristics from those of a metal to those of a semiconductor. In the compound (Figure 1.6) each unit cell contains two CuO_2 planes (I) and two CuO_x layers (II). The planes (I) are considered responsible for the superconducting phenomena. A description of this has been succinctly summarized from reference [9]. When all the oxygen has been removed from the layers (II) the material is an antiferromagnetic insulator with tetragonal structure [9]. When fully oxygenated ($x=7-\delta$) the Cu-O layers (II) oxygen bridges the Cu in one direction, effectively creating parallel Cu-O chains [9]. The

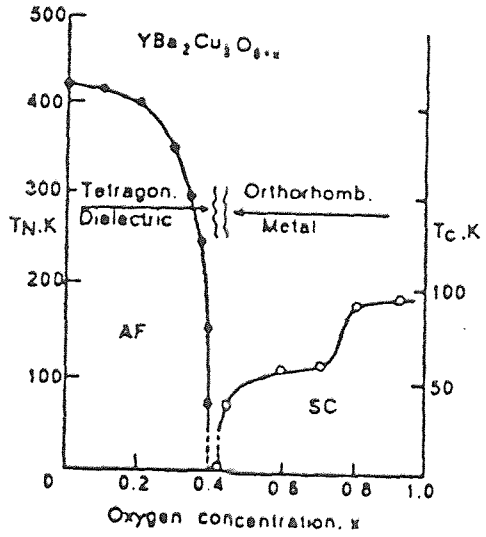

Figure 1.7 : Metal to insulator transition of $YBa_2Cu_3O_x$ as is deprived of oxygen ions

presence of these chains elongates the b lattice parameter (in the chain direction) so that it is longer than the a parameter and the entire structure is orthorhombic. An increase in oxygen content in the layers (II) results in an increase of carriers (in this case holes) in the planes (I). As x is varied, we see that chain ordering in the structure is accompanied by a transition from orthorhombic to tetragonal. It is surmised that the doping and superconductivity of $YBa_2Cu_3O_x$materials is due to the transfer of electrons from the CuO_2 planes (I) to the Cu-O chains (II) [9] . Figure 1.7 illustrates the tendency of the material to become increasingly 'insulator'-like as it is deprived of oxygen.

CHAPTER 2

PHOTOINDUCED EFFECTS

2.1 Background

In semiconductor materials, the absorption spectrum generally consists of one or more discrete lines and a continuous absorption band at higher frequencies [10]. The lowest frequencies absorbed (into the discrete energy bands) are capable of exciting an electron into a higher state in the field of the hole from which it originated. The field surrounding the hole creates a series of bound states for the electron. These centers of excitation, known as excitons, move throughout the lattice giving up some energy to produce phonons (quantized lattice vibrations) such that the sum of the exciton and phonon momenta is equal to zero. Therefore the selection rules governing optical transitions are satisfied.

However, higher frequencies absorbed into the continuous absorption band will produce free electrons and positive holes. Consequently, in the presence of an applied field, photoconductivity may occur [10, 11, 12]. Absorption in the exciton band does not cause photoconductivity, except when thermal energies from the lattice are great enough to promote the excited electron into conduction levels before their subsequent annihilation by holes. Photoconductivity (PC) is fairly common and quite well documented for semiconductors. Some semiconductors such as amorphous silicon also exhibit persistent photoconductivity.

Although photoconductivity is present in oxygen deficient $YBa_2Cu_3O_x$ its mechanisms differ from those of the traditional materials described above. In addition to

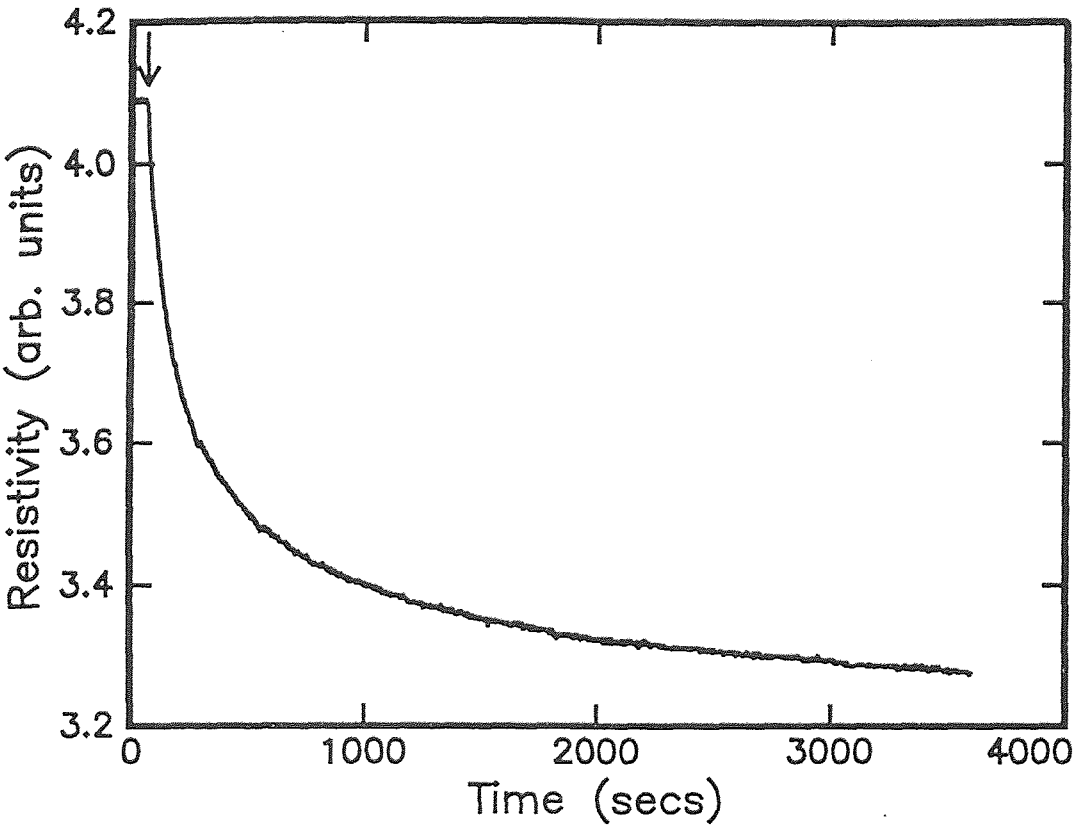

Figure 2.1 : Typical excitation time of PPC/PISC

PC, $YBa_2Cu_3O_x$ also exhibits persistent photoconductivity (PPC) in which the state of PC persists at low temperatures for days [9]. The activation time constants for this induced state vary from an hour for thin films (Figure 2.1) to mere seconds for single crystal samples [13] $YBa_2Cu_3O_x$ also exhibits photoinduced superconductivity (PISC) in which the characteristic T_c of the material under test is increased an amount which is dependent on the stoichiometry of the sample. In this state, the material is not only in an improved conducting state as in PPC but also is induced into its superconducting state. The material effectively becomes a superconductor at a higher temperature (Figure 2.2) These characteristics have been experimentally

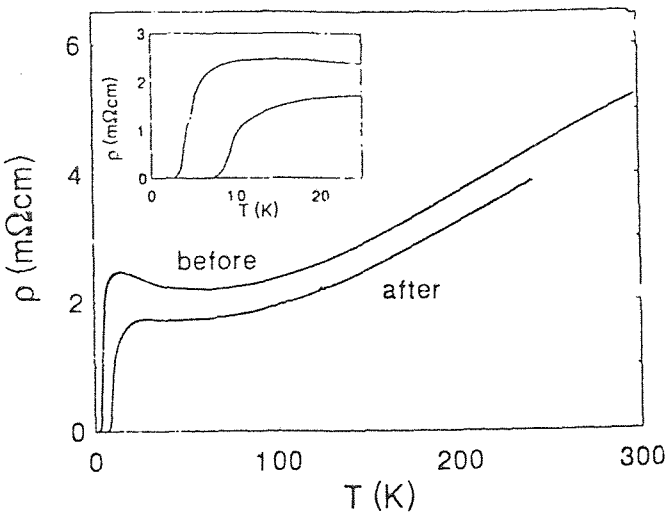

Figure 2.2 : T_c is changed by photodoping

observed under differing conditions and for various stoichiometries, but the mechanism(s) responsible is/are still under debate. However, it is clear from experiments [14, 9, 15, 16, 17, 18] that oxygen content plays an important role PPC and the PISC states of $YBa_2Cu_3O_x$.

2.2 Effects in $YBa_2Cu_3O_x$

When a sufficiently intense light pulse whose energy exceeds the superconducting energy gap interacts with a superconductor, the light pulse interferes in some way with the Cooper paired electrons (heats the sample above T_c and directly dissociates paired electrons) and hence destroys the superconductivity.[19] However, for high transition temperature copper oxide superconductors, experimental evidence[17, 20, 21, 13] indicates that the interaction of the light pulse with the superconductor can *enhance* the copper oxide's superconducting properties as measured by the material's transition temperature T_c, enhanced conductivity, and diamagnetism.

Various groups have studied the PPC/PISC effect using electrical resistivity, Hall effect, photoconductivity techniques, diamagnetism measurements, and x-ray scattering.[17, 20, 21, 13, 22]. Several possible mechanisms have been proposed to explain PISC, the first being defects in the high T_c materials. Second, polaronic type excitations which trap photoexcited electrons and prevent recombination of electrons and holes. Others proposed mechanisms include photoinduced diffusion of oxygen, photoinduced charge transfer in the CuO_2 planes, and electronic phase separation.

2.2.1 Charge Transfer Model

Kudinov et. al [9, 16] established the existence of a photoinduced transition from an insulating to a metallic state as well as photoinduced superconductivity in $YBa_2Cu_3O_x$ films. In addition, a persistent diamagnetic moment of the photoinduced state, which is indicative of a superconducting phase, was observed. The observed persistent photoinduced conductivity persisted for hours even at room temperature. The authors have suggested that the long lifetime could be due to the formation of a long-lived localized structural distortion around the photogenerated electron (polaronic structure). In recent work, Bud'ko et. al and Kudinov et. al[17, 20] used a variable wavelength excitation source to study the spectral dependence of the PPC response. The observed PPC efficiency curve was numerically fit to six Lorenzian lines throughout the visible range.[23] If a Mott-Hubbard model is used, the six peaks of the PPC spectra can be assigned to electron transitions in the CuO_2 planes corresponding to photoinduced charge transfer between the conduction band and the upper Hubbard unoccupied subband. The relaxation of PPC can be described by a thermally ac-

tivated process with an energy barrier of about 1 eV. As will be described in this chapter, we attribute these spectral peaks to Cu-O *chain* excitations in which electrons are trapped at oxygen vacancies (F-centers).

Oxygen Diffusion Model

It is well established that the T_c of quenched $YBa_2Cu_3O_x$samples slowly increases over time.[24, 25] In the slow annealing process which leads to an increased T_c, the sample composition is not altered (oxygen is neither added nor removed), but the location (ordering) of the oxygen in the lattice changes. In these samples, oxygen reordering during annealing induces a transfer of holes to the CuO_2 planes and a commensurate increase in T_c. In the proposed photoassisted oxygen ordering mechanism, illumination of semiconducting or partially superconducting material induces the required reordering of oxygen for charge transfer of holes to the CuO_2 planes and a superconducting transition. After photoexcitation, the PISC decays over time scales of days as the oxygen thermally diffuses bask to its initial configuration. However, Hall and lattice parameter measurements [15, 22, 21] strongly suggest that PISC is not due to oxygen reordering. Nieva et al. [21] conclude that oxygen ordering may be ruled out as a PISC mechanism because the electrical resistivity and Hall coefficient evolve in opposite ways for PISC samples and quenched samples (in which oxygen ordering is thought to occur). Likewise, the results of Hasen [15] and Lederman [22] show that the oxygen diffusion model is not correct: At low oxygen concentrations the PPC is greatly enhanced. In the oxygen diffusion model, the magnitude of the effect should be small for low oxygen concentrations.

Electronic Phase Separation Model

In the electronic phase separation[13, 26] model for PISC in crystalline samples, the photogenerated carriers are initially homogeneously separated. Subsequent to the photoexcitation, the carriers phase separate into clumps of metallic and insulating regions. Yu et al.[13, 27] interpret their observed minimum in photoresistance versus temperature in terms of disconnected metallic-superconducting regions separated by insulating regions. The observed minimum in resistance is due to the superconducting phase while the increase in resistance at low temperature is due to the 'series resistance' of the insulating regions. This interpretation is further supported by photoinduced absorption measurements which correlate infrared active vibrational modes (IRAV) with Raman modes of the *metallic* phase.[28] This correlation indicates the formation of metallic regions and metallic screening of phonon modes consistent with the supposition of phase separation.

2.2.2 Defect Model

Conceptually, PPC/PISC can be viewed as 'photodoping' a High T_c parent compound analogous to chemical doping of a material from an insulator to metal. In the case of $YBa_2Cu_3O_x$, this photodoping is analogous to increasing the oxygen context from $YBa_2Cu_3O_6$ to $YBa_2Cu_3O_{7-\delta}$. Subsequent to photoexciting a nonsuperconducting high T_c material (*e.g.* oxygen deficient $YBa_2Cu_3O_x$), one photoexcited charge species (electrons) is trapped while the other species (holes) contributes to the transient conductivity. If the transient carrier density were high enough, a transition from insulator to metal would occur. Presumably, if the charge carriers could form Cooper

pairs, a superconducting phase would form. The effect decays as photoexcited holes and electrons recombine.

It has been suggested that defects (most likely oxygen vacancies in the case of $YBa_2Cu_3O_x$ [29, 17, 15]) potentially play an important role in the PPC/PISC mechanism. The model as proposed by Hasen et al.[15] is similar to an existing model DX centers in GaAs.

> During illumination a photon creates an electron-hole pair. The electron can be trapped in an oxygen vacancy in the CuO_x chains layer where normally and O^- ion would be located in a fully oxygenated sample. The trapping of the electron causes a lattice distortion which results in a large energy barrier impeding the reverse recombination with the hole. The hole in turn is transferred into and extended state in the CuO_2 plane, thus enhancing the conductivity. As a result, the electron-hole pairs are only able to recombine at a high enough temperature for the electron to be thermally activated out of this self-trapped well. [15]

Clearly, if defects are important to the PISC, then the luminescence spectra of High T_c superconductors is one technique which might provide insight into the nature and dynamics of the defects. Certainly the results of the luminescence studies become easier to interpret and the conclusions drawn from them become more rigorous if the luminescence is intrinsic to the superconductor, i.e., if the luminescence corresponds to defects or traps in the copper oxide superconductors and is not contaminants (Y_2O_3, Y_2BaCuO_5), or grain boundaries. In this thesis work, we independently conclude that oxygen vacancy defects play a fundamental role in the PPC/PISC mechanism.

We identify the oxygen defects as F centers (an oxygen vacancy which traps two electrons) or F^+ (an oxygen vacancy which traps two electrons) centers rather than DX centers. Also, the correlation between the peaks observed in the luminescence spectra and those observed in the wavelength dependence of PPC suggest that the photogeneration of charges and their annihilation via luminescent recombination occur in the same level (Cu-O chains) of the $YBa_2Cu_3O_x$ crystal. Previous models had assigned the peaks in the PPC excitation spectrum to charge transfer in the CuO_2 planes. In addition, photoluminescence and infrared spectroscopy are used to characterize the energy levels of the defects.

CHAPTER 3

EXPERIMENTAL TECHNIQUES

3.1 Resistance Measurements

Three primary methods which will provide insight into a possible defect mechanism of PPC/PISC in $YBa_2Cu_3O_x$ are photoconductivity, photoluminescence and hall measurements. A description of each method and the information they are expected to yield follows.

Real time resistivity measurements are done using a typical four-point probe technique. Figure 3.1 shows a typical measurement configuration. A known current is passed through a channel and the subsequent generated potential through a portion of the channel is measured allowing calculation of the resistance. For thin samples with a thickness W smaller than either dimension a or d, the resistivity of the sample is given by

$$\rho = V/I \times W \times CF \qquad (\Omega - cm)$$

where CF is a tabulated geometry based correction factor. Curves providing this 'fudge' factor are readily available in many texts [30]. For our purposes the relative change in the resistance rather than the resistance itself is the value of interest.

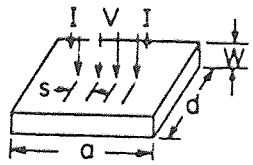

Figure 3.1 : Typical geometry for 4 point resistivity measurements

Monitoring the photoconductivity allows us to determine the rate and degree of 'excitation' to the photoinduced state as well as any subsequent changes brought on by the introduction of other variable to the measurement system.

3.2 Photoluminescence Measurements

Photoluminescence measurements [14] allow a more complete picture to be formed. In semiconductors photoluminescence occurs when an excited electron decays into a lower state and emits the excess energy in the form of a photon. Relative intensities of photoluminescence as a function of incident photon energies within the spectrum are indicative of the population densities of those excited states and the quantum efficiency. Thus when a probe in the form of a low intensity chopped laser beam is applied, a measure of the number of states available to trap these excited electrons is obtained for a *particular* energy. As we change system conditions, changes in the number available energy states are reflected in the photoluminescent intensity. In this manner, the photoluminescence spectra of the superconductor $YBa_2Cu_3O_x$ provides a means of determining the energies of available empty states as well as the relative occupancy of those states while experimental conditions are varied.

3.3 Hall Measurements

Hall measurements [18] provide direct measurement of the carrier type and concentration and, in conjunction with the resistivity, yield the mobility. The Hall effect occurs when a substance carrying a current is subjected to a magnetic field perpendicular to the direction to the current. Physically, we see (Figure 3.2) that a current flowing

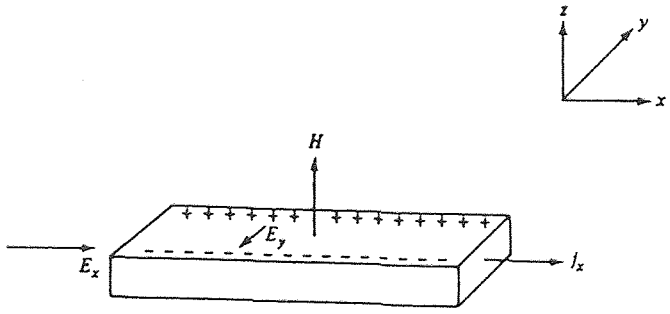

Figure 3.2 : Geometry for Hall calculations

in the x-direction and an applied magnetic field in the z-direction produces a potential gradient across the sample in the y-direction. Mathematically the relationship is expressed as follows:

$$\nabla V_H = -R_H j H$$

where

$$\nabla V_H \Rightarrow \text{(the transverse potential gradient)} = -E_H$$

$$E_H \Rightarrow \text{Hall field}$$

$$j \Rightarrow \text{current density}$$

$$H \Rightarrow \text{applied magnetic field}$$

$$R_H \Rightarrow \text{Hall coefficient}$$

If the sample is a rectangular solid of width a and a thickness b and the distribution of current is assumed to be uniform throughout the sample, the above equation can be rewritten in terms of the total current I, the Hall voltage V_H and the dimensions of the sample.

$$\nabla = V_H/a = -R_H I H/(ab)$$

$$V_H = -R_H I H/b$$

The effect can be visualized by considering the particle nature of conduction. A stream of charged particles will flow longitudinally through the sample without deviation in the absence of a magnetic field. On application of a magnetic field, the current carriers experience a force $e(v \times H)/c$ and are swept to the edges of the sample. This process continues until the field due to the nonuniformity of charge distribution on the sample exerts a force equal to the deflecting force of the magnetic field. This condition for a steady state is met when the force exerted by the transverse electric field due to the charge build up at the edges of the sample equals that of the deflecting force of the magnetic field. From the measurement of the Hall coefficient, the carrier concentration and mobility can be determined. The equation

$$R_H = (3\pi/8)(1/pec)$$

where p is the carrier concentration allows the extraction of p from a measurement of V_H through the relation

$$R_H = V_H b/IH$$

as obtained from the transverse potential gradient. It is easily apparent that variation in V_H will be a direct consequence of variation in carrier concentration. Manipulation of Ohm's Law

$$j = \sigma E$$

where

$$\sigma = qe^2\tau_h E/m_h$$

in conjunction with the definition of mobility

$$\mu_h = d\tau_h/m_h$$

yields the familiar expression

$$\mu_h = \sigma/ne = 1/ne\rho$$

relating the resistivity and the mobility. Further manipulation yields the form

$$\mu_h = c(\mid R_H \mid /\rho)$$

which provides a value for the mobility from two measured quantities.

CHAPTER 4

SAMPLE PREPARATION

4.1 Fabrication

4.1.1 Deposition

Thin films of $YBa_2Cu_3O_x$ with various stoichiometries were prepared for the investigation using Pulsed Laser Deposition (PLD) with the appropriate post-ablation annealing. PLD can be simply described as removal of a solid from a target and deposition via a resulting plasma to a nearby available substrate.

Laser/Target Interaction

The described processes occur within a vacuum sealed chamber as illustrated in Figure 4.1. In general, as the laser beam hits the target photons are absorbed by the surface. The surface then becomes a molten layer which vaporizes. The vaporization process creates a recoil pressure on the liquid layer and the molten material is expelled towards the substrate.

This process for the UV Excimer laser and $YBa_2Cu_3O_x$ interaction has been succinctly summarized from Reference [31]. While the laser beam is at the surface of the target, the increase in surface temperature and ensuing formation of the molten layer is dependent on the optical penetration of the material, the thermal diffusion of the target, and the rate at which energy is injected into the system. The high temperatures at the surface cause emission of various ions and electrons as well as neutral atoms and molecules which have been dissociated from the bulk. Photoionzation of

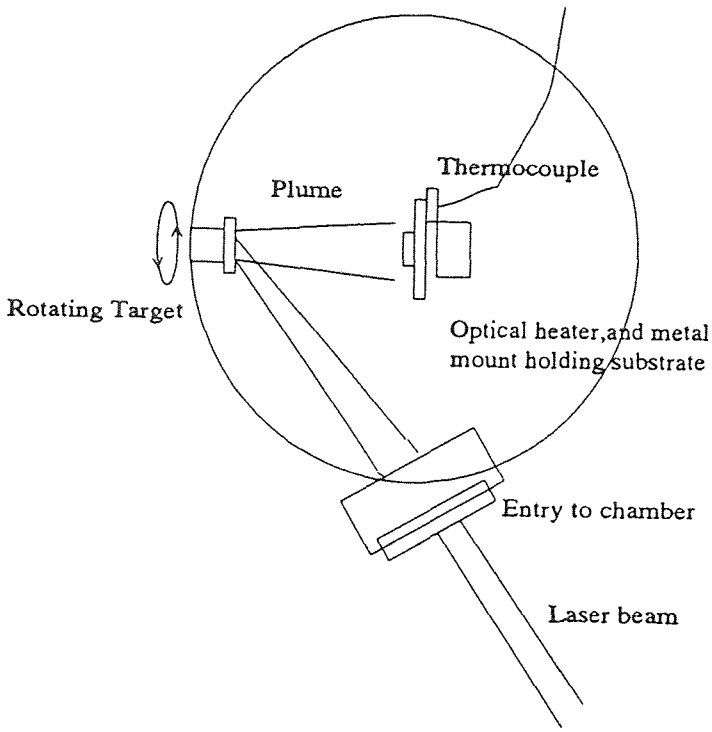

Figure 4.1 : Drawing of a basic chamber and locations of target and substrate

this evaporated material by various processes leads to the formation of an expanded plasma above the surface [31]. It then expands away from the target surface. This 'plume' of evaporated material is characterized by a specified peaked distribution function [31] contrary to the expected thermal distribution. The difference in these angular distributions indicates that the precise combination of mechanisms for removal of material from the surface is more complex than indicated. Various models have been proposed for this process [32, 33, 34, 35, 36] which provide a basic grasp of the picture but many questions remain unanswered [31]. There is also found [37] to be a variation in stoichiometry of the plume dependent on the angle θ away from the target normal. Consequently, there is an small nonstoichiometric component in PLD multicomponent materials. From this description, the importance of substrate location in the plume, energy density at target surface and reactive gas content in the chamber play an important role in the final composition and quality of the film. The particular conditions under which our samples were fabricated are described in the following section.

Chamber Conditions

The Ft. Monmouth ARL- Physical Sciences Division currently houses a laser ablation facility and operates a KrF (248 nm) Excimer laser. For these samples a typical repetition rate of 10 Hz and energy density per pulse of 300 mJ was used. The beam enters the chamber via a quartz window and is focused on a rotating $YBa_2Cu_3O_x$ target. The rotation of the target prevents target melting and helps reduce the formation of clusters. Particulates vary according to operating efficiency of laser.

Adjustments of the operating frequency, oxygen atmosphere and focal point of the laser entry to the chamber have been varied on occasion to maintain the appropriate energy density of the plume at the substrate and a consistent deposition rate.

The substrate is mounted on a metal plate with silver paint to ensure good thermal contact and is heated optically from behind. With the use of a thermocouple attached to the metal plate and a controller, the substrate is heated to a predetermined temperature and the temperature is verified using a pyrometer. For this particular system, significant differences (10-20^{o}C) between controller indicated temperature (at the plate) and the pyrometer measured temperature (at the surface of the substrate) indicates poor thermal contact and mounting should be repeated. Another more obvious indication of poor thermal contact is visible color differences at the surface of the substrate. In either event, ensuing deposition will not be uniform and the resulting film quality will be poor; it is then generally advisable to remount the substrate. Deposition is done at 820^{o}C.

During deposition, the substrate should centered as close to zero degrees θ from the target normal and be within the plume. Some groups [38] position their substrate outside of the plume to enhance thickness uniformity and decrease surface roughness. However, these gains are offset by the reduction of T_c and a possible departure from cation stoichiometry [38]. Damage can also be done to the film by placing the substrate too close to the target where a central blue region of the plume exists. The energy density of the plume is controlled by the partial pressure of oxygen present in the chamber during ablation. Films for the projects described in the remainder of the paper were ablated under an oxygen partial pressure of 100 mT$\pm$3 mT (except

when as previously described to aid in compensating for reduction in laser power).

After deposition, the chamber is flooded with oxygen to $\frac{1}{2}$ atm and is cooled to $800°C$ over a period of 10 minutes (to allow oxygen ordering) and to $400°C$ over the next 20 minutes. At this point the chamber is allowed to cool to room temperature and the film is removed. As ablated films are generally fully superconducting with T_c approximately $90°K$. We have observed that faster cooling does not allow time for proper oxygen ordering and results in a lower T_c.

4.2 Post Deposition Annealing

The primary effect of annealing is to create the desired stoichiometery in the sample through oxygen removal and reordering. Initial annealing attempts utilized a real-time resistance monitoring system a full oxygen atmosphere anneal. Peak temperatures were chosen from extrapolation/interpolation of initial resistance versus temperature measurements and tended to be chancy at best. Samples were bonded in a ceramic in-line package a placed in a quartz tube under vacuum within a simple ceramic furnace with a constant flow of O_2 through the tube. It was observed that hot zones within the furnace gave uneven annealing and that targeting particular resistances (indicative of specific oxygen contents) did not provide reliable and consistent results.

Thus, a further literature search revealed thermogravimetric studies of enthalpy for oxidation of $YBa_2Cu_3O_x$[39]. Using a series of isocompositional lines on a plot of $log\ P_{O_2}$ versus reciprocal temperature (Figure 4.2 [39]) and a plot of oxygen contents at various temperatures for a series of different oxygen atmospheres (Figure 4.3 [39])

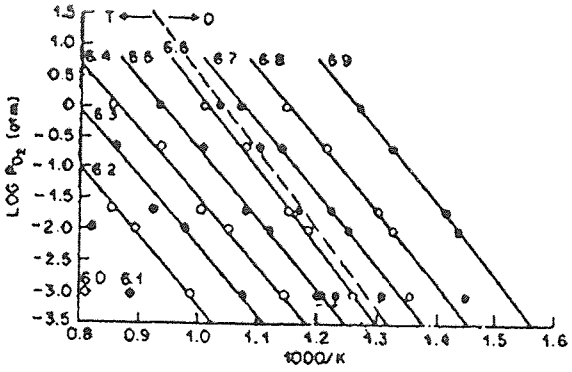

Figure 4.2 : Isocompositional lines for $YBa_2Cu_3O_x$

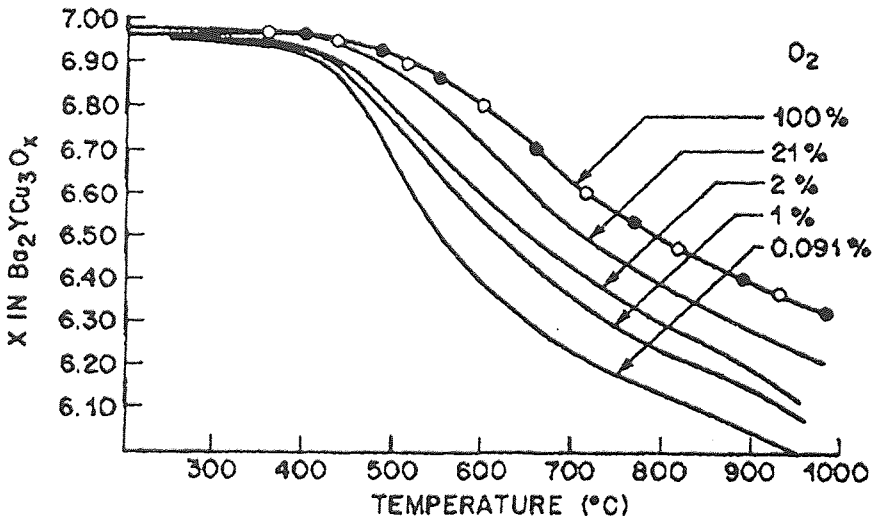

Figure 4.3 : Oxygen content versus temperature for $YBa_2Cu_3O_x$ in different partial pressures of oxygen

we were able to estimate appropriate annealing temperatures for our desired stoichiometries. In this vein, samples were placed on a platinum shelf in a quartz tube. The tube was then inserted into a platinum/alumina muffle powered by a current source and regulated by a thermocouple close to the sample shelf and an Iveron programmable controller. The meticulously clean tube, boat and sample were subject to a partial atmosphere of O_2 in a balance of N_2 throughout the anneal cycle.

This annealing set-up was used until the muffle cracked. Because the manufacturer no longer fabricates these alumina coated platinum muffles, a reconfigured furnace system was derived. In this new arrangement, the same controller and current source are used in conjunction with a standard ceramic tube furnace (a large resistor of approximately 30 Ω with a hollow center). The effect of this substitution was a greater susceptibility to uneven heating from a smaller 'hot spot' at the center of the furnace and the increased probability of sample/thermocouple/'hotspot' misalignment. Process errors result in visible discoloration of all or portions of the sample. These 'burnt' areas are the result of temperatures higher than 800^oC at which the $YBa_2Cu_3O_x$ decomposes into various cuprates [40].

Annealing time was determined based on the recent results of Tidrow showing oxygen diffusion time through $YBa_2Cu_3O_x$ thin films [41]. Tidrow et al. reveal that O_2 diffuses along grain boundaries and is aided by material defects in the a and b planes. Based on the authors' work and results, necessary annealing times were estimated to be on the order of 20 to 30 minutes and chosen to be on the order of an hour. For thin films fabricated in the manner previously described, this was deemed sufficient. However, for future work, it should be noted that for larger grains or no

grain boundaries (single crystals) O_2 diffusion rates and therefore annealing times are significantly different [40].

4.3 Characterization

After annealing, the samples are characterized by with transition temperature measurements and x ray spectra. The critical temperature of the sample is determined using an AC probe and cryostat system. As a function of temperature the intensity of sample response (proportional to resistivity) is determined. The quality of the final product can also be determined from this T_c measurement. The width of the transition ('Full Width Half Max' of the first derivative of the curve) should be quite narrow. A width of $\frac{1}{2}$ to 2 Kelvin is considered excellent and widths on the order of a few degrees are generally acceptable.

The x ray spectra of the film is used to determine the c axis lattice spacing. This parameter then allows us to calculate the oxygen content of the film and estimate a critical temperature from previous empirical studies [42, 43]. Interference of x rays due to scattering from various sets of parallel planes of atoms yields relative maxima and minima. Waves scattered from two successive atoms within a plane will be in phase and thus interfere constructively, independent of the wavelength if the scattering angle equals the incident angle. Waves scattered at equal angles from atoms in two different planes will be in phase if

$$2dsin(\theta) = m\lambda$$

where m=integer is satisfied. This condition, known as the Bragg equation, in combination with the measurement of scattered intensity as a function of incident angle

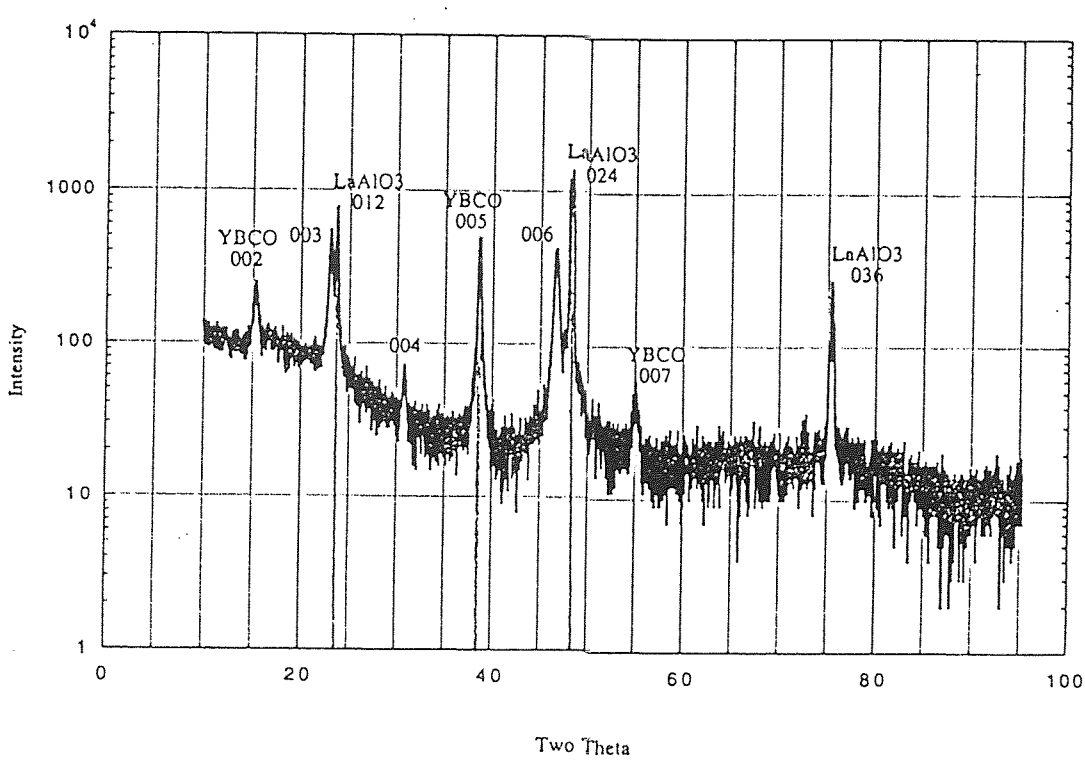

Figure 4.4 : Typical x ray spectra

(of x rays) produces empirical values for the 'd-spacing' or c axis parameter of the crystalline thin film. Figure 4.4 shows a typical x ray spectra with the Miller indices of the $YBa_2Cu_3O_x$ and $LaAlO_3$ peaks indicated. For the sample shown

$$d = (1.511\mathring{A} \times 5)/(2 \times sin(2\theta/2))$$

Note that a slight offset due to lag between initiation of x ray and automated data acquisition system, peak locations have been calculated with respect to known $LaAlO_3$ peaks. Therefore we see that d=11.515Å and from Reference [43] x=6.72.

4.4 Patterning

Films were patterned using standard UV lithography techniques. Photoresist is spun onto the film before a shadow mask is aligned and the remainder of the film is exposed to ultraviolet light. After exposure, the exposed resist and $YBa_2Cu_3O_x$ under it are etched. The final product is a patterned area of the thin film and exposed substrate. Choices of patterning geometries were made based on physical limitations of the systems and are described in the following paragraphs.

Two experimental set-ups were used for different phases of the experiment. Both the New Jersey Institute of Technology (NJIT) and Army Research Laboratory Physical Science Directorate (ARL) at Fort Monmouth NJ facilities were utilized. Samples produced for photoluminescence measurements in the NJIT lab differed in geometry from those produced for the experiments incorporating the Hall Effect which were run in the ARL location. For the NJIT set-up, consideration of physical measurement limitations forced the use of unpatterned films. It had been found that patterned

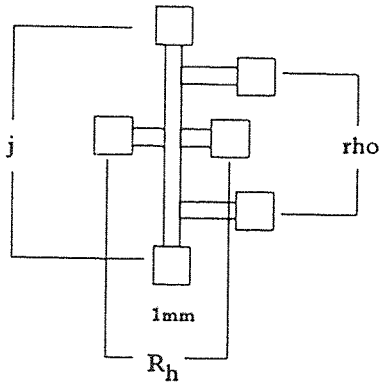

Figure 4.5 : Illustration of patterning for Hall measurements

films left substrate material (Lanthinum aluminate) exposed to the impinging radiation. Consequently, the photoluminescence spectra collected from these samples was a combination of the $YBa_2Cu_3O_x$ spectra and $LaAlO_3$ spectra. Unpatterned samples allowed collection of pure $YBa_2Cu_3O_x$ spectra. All data shown is from this geometry, presenting only the effects of the $YBa_2Cu_3O_x$ photoluminescence without spectral contamination from the $LaAlO_3$.

Films for the ARL Ft. Monmouth set-up have been patterned (Figure 4.5) to allow for easy Hall effect analysis. A single channel forces current through it rather that allowing the current to travel in a meandering path through the least resistive areas of various domains in a thin film. Although homogeneity in the thin films is ideally strived for, this is not physically feasible in the PLD process (refer to previous description of PLD). However, the degree of nonstoichiometry and inhomogeneity within and across a film is too small to be of any appreciable significance in later calculations. For data comparison purposes, these separate sample geometries were chosen to maximize accuracy of data. Processing conditions for all samples are held constant (for a given stoichiometery), thus providing consistent samples for both equipment set-ups.

CHAPTER 5

PHASE I: EXCITATION

5.1 Apparatus

During the first phase of the experiment the de-oxygenated films are mounted in a ceramic dual inline package and the contacts wire bonded to the gold contacts on the sample. The package is inserted into a liquid helium vapor optical cryostat which permits cooling of the sample using either liquid helium or liquid nitrogen. The film resistance is measured using standard 4-point resistivity techniques while the photoluminescence is measured using a 0.25 m scanning grating monochrometer (spectral resolution 1nm) and a photomultiplier detector. The photoluminescence spectrum is measured by mechanically chopping a low intensity laser beam (30 mW, 476.2 nm, 4mm spot size) and using phase sensitive detection to measure the photoluminescence spectrum as the monochrometer is scanned. A yellow glass filter is placed in front of the monochrometer entrance slit to reject stray laser light. The monochrometer, photomultiplier detector, and 4-point resistivity electronics are interfaced to an automated data acquisition system.

5.2 Results

Figure 5.1 shows a typical resistance versus temperature curve of an insulating $YBa_2Cu_3O_{6.4}$ film before and after one hour of illumination with 4 W (all lines) from an Argon Ion laser. During the 4 W illumination, the sample is immersed in liquid nitrogen to maintain the sample at approximately a constant temperature. A constant tempera-

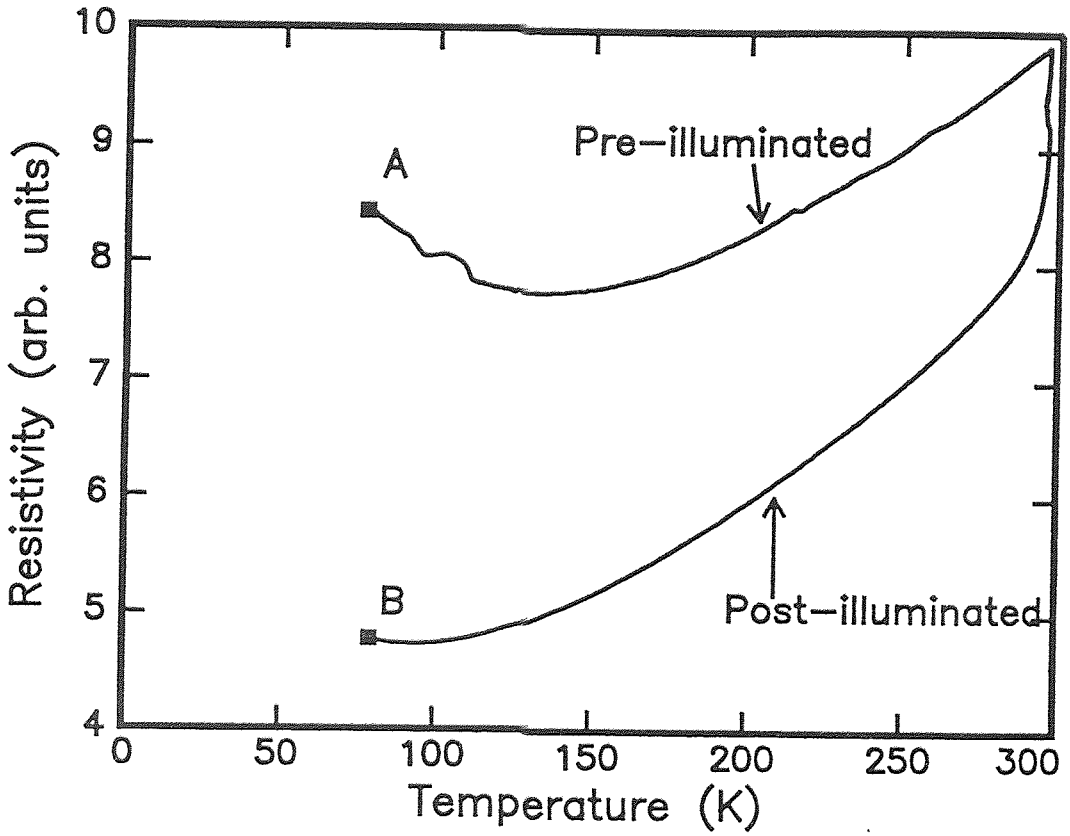

Figure 5.1 : Typical resistance versus temperature curve of $YBa_2Cu_3O_{6.4}$ before and after one hour of illumination with 4 Watts from and Argon Ion laser

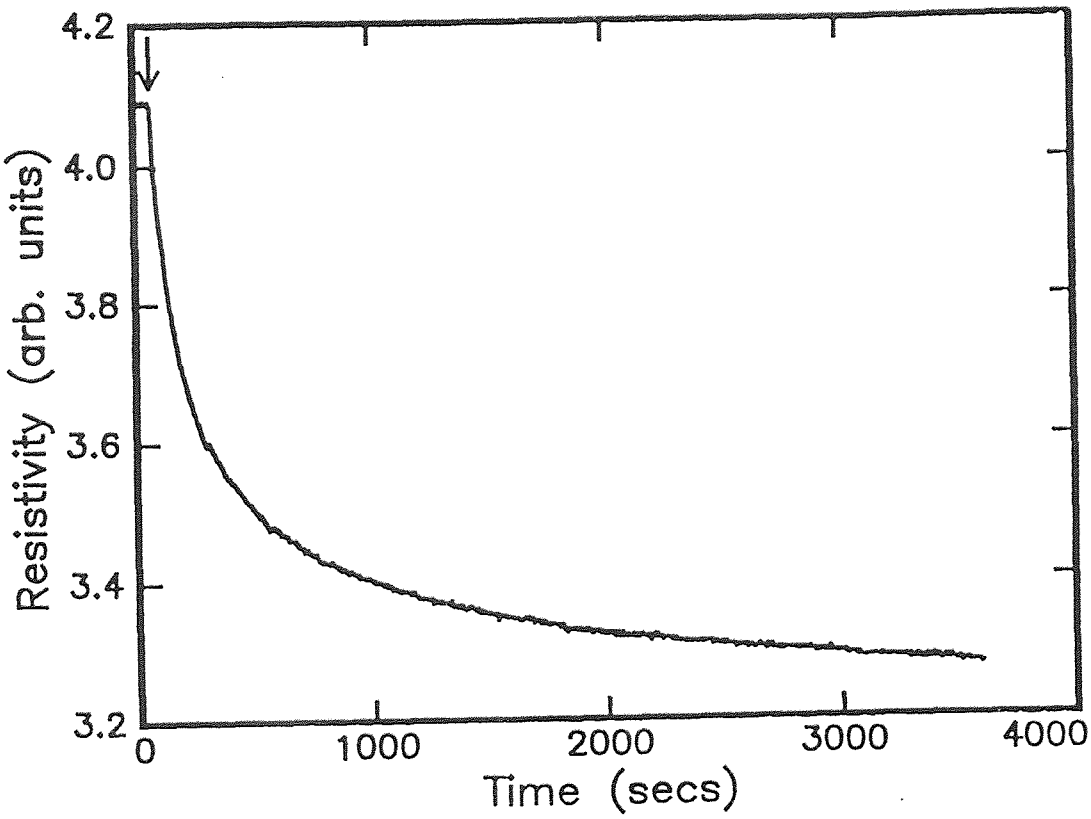

Figure 5.2 : Electrical resistance of the film during illumination of 4 Watts Argon Ion light

ture ensures that any observed changes in photoluminescent intensity are due to the photoinduced state and not due to temperature induced changes in the defects' luminescent properties. The illuminated sample's resistivity returns to its unilluminated value after about 33 hours at room temperature. Figure 5.2 shows the electrical resistance of the film as a function of time during the illumination with 4 W of light with the sample immersed in liquid nitrogen. The decrease in resistance is nonexponential.

The room temperature and 77 $^{\circ}K$(unilluminated) photoluminescence spectra of an insulating $YBa_2Cu_3O_{6.4}$ film are shown in Figure 5.3. The excitation light for photoluminescence is keep at 30 mW to minimize the changes in photoinduced conductivity during the luminescence data acquisition. There are narrow luminescent

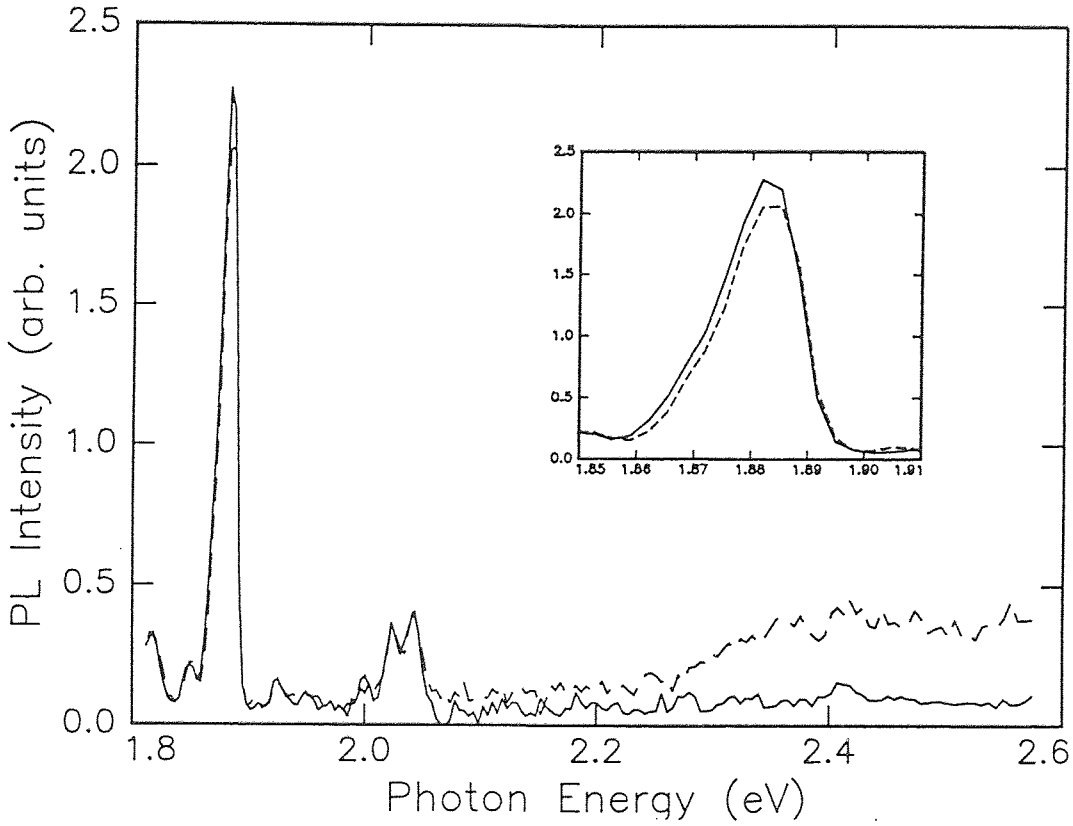

Figure 5.3 : Photoluminescence spectra of x=6.4 sample at room temperature and $77^{o}K$

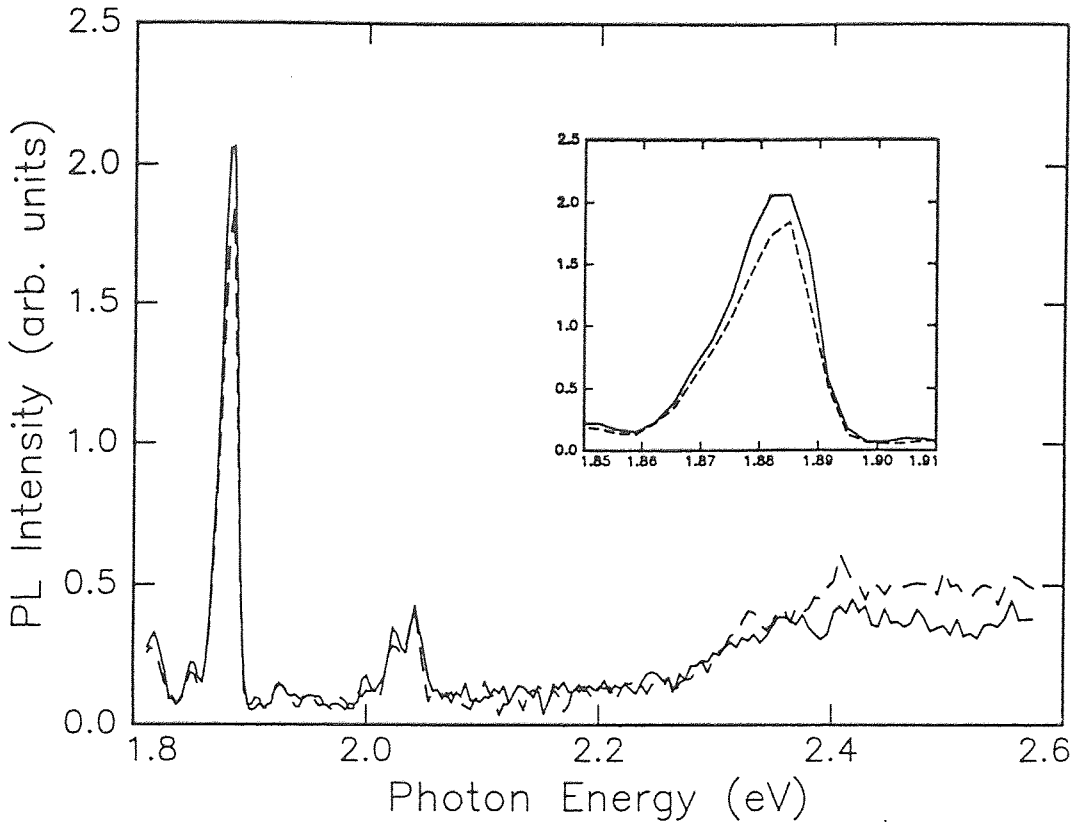

Figure 5.4 : Photoluminescence intensity at $77°K$ after 1 hour illumination

peaks at 1.88 eV, 2.03 eV while a broad feature near 2.4 eV appears upon cooling. The 77 $°K$ photoluminescence spectrum at points A and B of Figure 5.1 (before illumination and immediately after illumination) are shown in Figure 5.4. After 1 hour of illumination, there is a drop in the luminescent intensity at 1.88 eV and an increase at 2.4 eV while the photoluminescent intensity at 2.03 eV remained constant.

These measurements were repeated for superconducting $(7-\delta)$ and partially superconducting (6.6) films. For unilluminated films at 77 $°K$, the overall photoluminescent intensity of the partially superconducting and superconducting samples decreased, compared to the insulating samples, by a factor of 100. The ratio of the 1.88 eV to 2.4 eV intensity peaks changed as the oxygen content increased. For the

insulating films, this ratio was $PL_{1.88}/PL_{2.4}=10$ while for the partially superconducting and superconducting samples, the ratio was about 1 and 0.2 respectively. Upon 1 hour illumination, the partially superconducting sample showed a small decrease in the 1.88 eV luminescence and a small increase in the 2.4 eV luminescence. No perceptible change is observed in the luminescence spectra of superconducting samples. For unilluminated samples, the intensity of the 1.88 eV peak decreases with increasing oxygen content (decreasing population of oxygen chain vacancies). Upon 1 hour illumination, the magnitude of the change in photoluminescent intensity decreases with increasing oxygen content.

5.3 Discussion

Since the superconducting copper oxides are opaque in the energy range of the escaping luminescent light (absorption coefficient $10^4 - 10^6$ cm^{-1}), the detected luminescence originates from only the first few microns of material; luminescence from deeper in the sample is strongly attenuated. It has been asserted that luminescence can not be observed from the superconducting phase of copper oxides (in analogy with a metal) since there is no band gap of sufficient magnitude to trap the radiation-induced charges. Thus luminescence has been touted as a sensitive method for determining the amount of impurities in a superconductor.[44, 45, 46]

Table 5.1 summarizes previous studies of luminescence of superconducting $YBa_2Cu_3O_x$ subsequent to excitation by electron beams (cathodoluminescence), synchrotron radiation, and x-rays. All of the studies show a weak luminescence of the superconductor. As seen from Table 5.1, the most common luminescence peaks are about 1.9, 2.4, 2.9, 3.35, and 3.6 eV with corresponding thermal activation energies in the 0.2 to 0.5 eV

Table 5.1: Characteristic Photoluminescence Peaks in $YBa_2Cu_3O_x$

Author	Technique	Lum. Peaks (eV)	Activation Energy
Roth[47]	x-ray TSL	3.65	.16, .42eV
		2.9	
Cooke[46]	x-ray TSL	1.88, 3.63	.429eV
			.265eV
			.290eV
Lushchik[48, 49]	cathodo	3.355	.024eV
Fugol[50]	cathodo	3.36, 2.9	
		3.6,2.9,2.4	
Stankevich[51, 52]	photo, cathodo	2.9	
Popova[53]	cathodo	3.36, 3.31	
Eremenko[54]	cathodo	3.36, 3.31	
Andreev[55]	cathodo	2.75, 1.91	
Luff[56]	cathodo	3.65, 2.58, 2.7	

range. Some features, such as the 1.88 eV peak, are narrow while others, such the 2.4 eV feature, are broad. These activation energies are the same order of magnitude as measurements of the thermal activation energy (.935 eV) for the decay of PISC.[17] Typical trap capture rates for luminescence are in the 10^6 to 10^9 sec^{-1} range. From luminescence measurements, the density of defects were estimated by Roth[47] to be at least 1 of every 10^4 lattice cells assuming unity quantum yield. If the quantum yield is closer to the $10^{-3} - 10^{-4}$ as estimated by Lushchik[48], this suggests that *the density of defects may approach one defect per unit cell.*

Some previous studies have concluded that the photoluminescence from superconductors is intrinsic. In analogy with simpler oxide systems such as Al_2O_3, MgO, and BeO, Cooke et. al[57, 47] suggested that F centers (two electrons trapped at an oxygen vacancy) and F^+ centers (one electron trapped at an oxygen vacancy) are responsible for the two peaks (1.88 eV, 3.63 eV) in luminescence spectra of $YBa_2Cu_3O_x$ superconductors. By correlating photoluminescence with electrical measurements of PISC, it will be apparent if these hypothesized luminescent defects are a fundamental component of the PISC mechanism.

We suggest that defects may be intimately related to the PISC mechanism: *peaks in the PISC efficiency as a function of excitation wavelength [17, 20] correspond to well-known photoluminescence peaks in* $YBa_2Cu_3O_x$ (See Figure 5.5). Figure 5.5 shows the numerical fit to the wavelength dependence of PPC[20, 17] with the reported photoluminescence energy peaks indicated. Clearly, there appears to be a strong correlation between the two spectra over the range of reported PPC efficiency data. The wavelength dependence of PPC reported by References [20] and [17] was

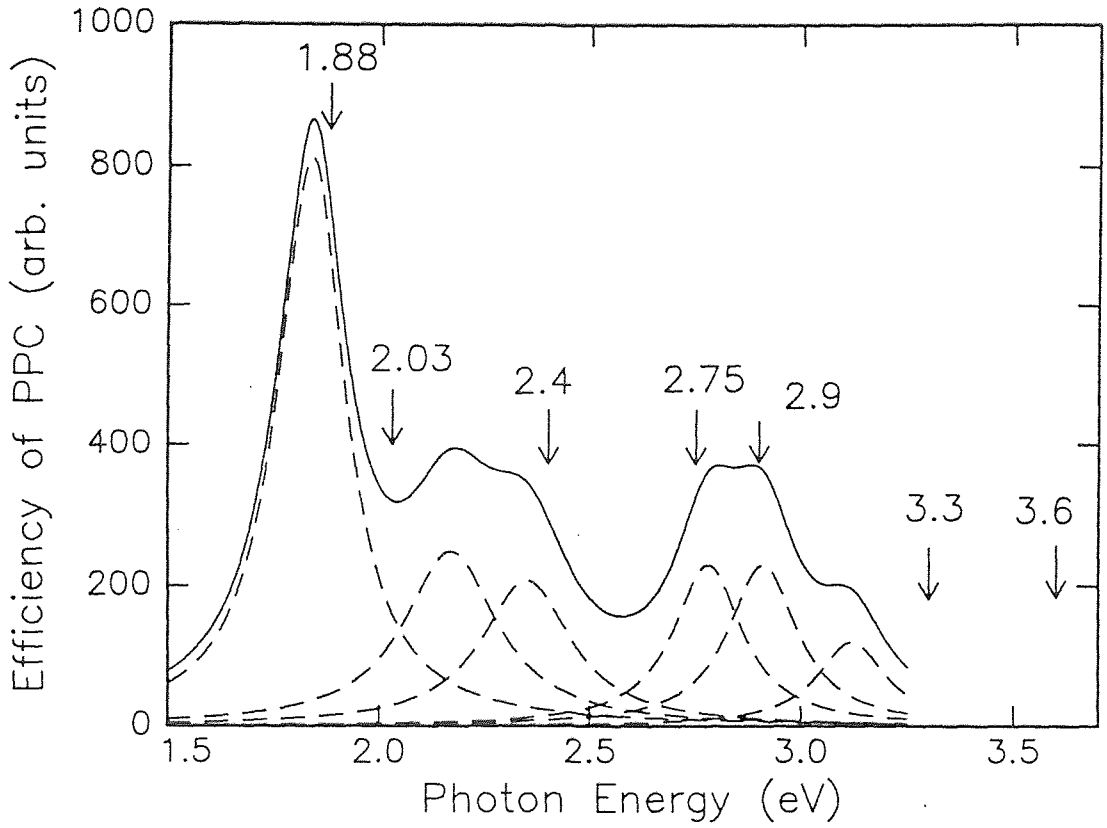

Figure 5.5 : Correlation of reported PL peaks and PPC effeiciency

limited by a range of 1.4 to 3.2 eV. The limited range might explain why the photoluminescent peak at 3.3 eV is displaced from the 3.1 eV PPC peak. It is not known if the photoluminescent peak at 3.6 eV corresponds to resonances in the PPC efficiency. As will be discussed below, the peak at 2.03 eV reported in this paper *can not be* attributed to the PISC/PPC mechanism. Experiments to extend the photoluminescent spectra to 4 eV are underway. Currently, we are limited by the wavelength range of our argon ion laser (514,488,476 nm excitation) which is being used as the luminescence excitation source. As with the work of Cooke et al. [57, 47], we assign the 1.88 eV peak to luminescence from F-centers (electrons trapped at oxygen vacancies) in the Cu-O chains.

Photoluminescence measurements with a modulated weak probing laser beam measure the number of available oxygen vacancies. Upon photoexcitation with a weak probe, some of the photoexcited electrons are trapped by oxygen vacancies. Since the probe beam (30 mW) is much weaker than the 4 W used to induce PPC, the average number of oxygen vacancies which are available to trap an electron has not been significantly altered during the 60 s luminescence measurement. However, by modulating the probing light, the resultant luminescence is also modulated. If a significant number of vacancies are filled (either by trapped electrons or by oxygen if the sample is not completely oxygen deficient), than there are fewer vacancies to trap the photoexcited electrons. Therefore, the photoluminescent intensity should decrease as the number of oxygen vacancies decrease. Our measurements on $YBa_2Cu_3O_x$ films with varying oxygen content which show a decrease in 1.88 eV photoluminescent intensity as the oxygen content is increased (number of oxygen vacancies is decreased)

from 6.4 (insulating) to 6.6 (partially superconducting) to $7 - \delta$ (superconducting) support this statement.

When the persistent conductivity state is induced, the luminescence spectra changes (Figure 5.4). Since the sample is maintained in liquid nitrogen during the 4 W illumination and the luminescence measurement, changes in the PL spectra can not be due to temperature changes. The spectra after illumination shows a decrease in the photoluminescence at 1.88 eV and a broad increase at about 2.4 eV. The peak at 2.03 eV does not change between the 'dark' and 'photoinduced' states. This suggests that the 2.03 eV peak is not correlated to the PPC/PISC effect and is therefore not related to the defect mechanism. The broad luminescence feature near 2.4eV may correspond, as it does in the PPC wavelength dependence (Figure 5.5), to two overlapping photoluminescence peaks. Figure 5.4, which shows the decrease in 1.88 eV luminescent intensity upon 4 W illumination, suggests that this decrease occurs since fewer vacancies are present to trap electrons in the photoinduced sample. By comparing Figs.5.3 and 5.4, the increase in luminescent intensity at 2.4 eV and decrease at 1.88 eV is consistent with a fewer number of available vacancies after 1hour illumination and the sample becoming more metallic. The concurrent changes in resistivity and photoluminescence spectra upon 4 W illumination imply that both changes are due the PISC/PPC state.

Previous studies of the PPC mechanism had suggested that the photoexcitation of electron-hole pairs occurs in the CuO_2 plane. In this charge transfer model,[17] the photoexcited holes stay in the CuO_2 plane while the photogenerated electrons transfer to the chain layers. Based upon our results, the relevant defects for PPC can

not be located in the CuO_2 planes. If the defects were in the planes, than one would not expect these defects to be present in metallic $YBa_2Cu_3O_x$ since the large number of free holes in the planes would annihilate the trapped electrons. For this reason, luminescence has been touted as a sensitive method for determining the amount of impurities in a superconductor.[44, 45, 46] Luminescence can not be observed in a metal since there is no band gap of sufficient magnitude to trap the photogenerated charges. However, photoluminescence as well as PISC persist *even for partially superconducting samples*. Therefore, if defects are important to the PISC mechanism, they must reside in the Cu-O chain layers so that trapped electrons are physically separated from holes in conducting CuO_2 planes. Moreover, the fact that PISC efficiency spectra and photoluminescence peaks are correlated suggests that the photogeneration of carriers and their annihilation via luminescent recombination *occur at the same location in the* $YBa_2Cu_3O_x$ *crystal*. Optical studies of the a-,b-, and c-axis charge dynamics in $YBa_2Cu_3O_x$ reveal a 1.75eV peak in the optical conductivity[58] which corresponds to charge-transfer of a hole between the Cu(2) $d_{x^2-y^2}$ and O(2,3) $p_{x,y}$ sites on the CuO_2 planes. The absence of 1.88, 2.1, 2.4 eV features in optical reflectivity measurements of $YBa_2Cu_3O_x$ and Gd_2CuO_4, which has no chain layers, implies that the spectral features observed in PPC/PISC and photoluminescence are *chain* excitations. Thus we suggest that the PISC mechanism is dominated by oxygen vacancy defects in the CuO chains at which the photogeneration and luminescent decay of electron-hole pairs take place.

As discussed above, one would not expect a large number of trapped electrons in a metal where a large number of free holes are present to annihilate the elec-

trons trapped at a defect. Since the PISC/PPC effect persists for hours even for partially superconducting samples (suppressed T_c), the defect model needs to consider the stability of the F-center upon photoexcitation. Two features stabilize the F-center and prolong the lifetime of the photogenerated carriers: lattice deformation around the trapped electron and physical separation of the electrons and holes. As with other materials with F-centers, one might expect that the lattice locally deforms around the trapped electrons. Lederman et al. [22] report that upon photoexcitation of $YBa_2Cu_3O_x$, the lattice parameters shrink indicating a more stable configuration. In addition, the large spatial separation between photoexcited electrons, which are trapped at oxygen vacancies in the Cu-O chain, and holes, which are in the conductive CuO_2 planes, implies a small overlap of their wave functions and therefore a lower probability for recombination of electrons and holes to quench the photoinduced conductivity. Therefore, the low photoluminescent efficiency in photodoped $YBa_2Cu_3O_x$ implies a long-lived state which is stabilized by lattice deformations and the physical separation of trapped electrons and conducting holes.

5.4 Summary

Photoconductivity and photoluminescence measurements on $YBa_2Cu_3O_x$ thin films strongly suggest a defect mechanism for persistent photoconductivity and photoinduced superconductivity in these materials. Oxygen vacancies in the Cu-O chains act as F-centers which trap photoexcited electrons and prohibit their recombination with photoexcited holes. The correlation between the peaks observed in the luminescence spectra and those observed in the wavelength dependence of PPC suggest that the

photogeneration of charges and their annihilation via luminescent recombination occur in the same level (Cu-O chains) of the $YBa_2Cu_3O_x$ crystal. Previous models had assigned the peaks in the PPC excitation spectrum to charge transfer in the CuO_2 planes. However, the defects which give rise to the PISC effect can not be located in the CuO_2 planes where the large number of holes would easily annihilate the trapped electrons and quench the photoinduced state. In the oxygen vacancy defect model, the 1.88eV level is assigned to the luminescence from electron-hole recombination at the defect site. The decrease in the 1.88 eV luminescence and increase in the 2.4 eV luminescence upon photoexcitation is a consequence of a decrease in the number of oxygen vacancies in the chain layers. The F-center is stabilized by (1) lattice deformation around the captured electron and (2) physical separation of the trapped electron in the chain layer and the conducting hole in the plane layer.

CHAPTER 6

PHASE II: QUENCHING

6.1 Introduction

Recall that in this model, oxygen vacancies trap photogenerated electrons so that electron-hole recombination cannot occur thereby allowing photogenerated holes to contribute to the carrier density. The effect decays as electrons are released from their traps and recombine with photogenerated holes. Our previous studies (discussed in the previous chapter) of photoluminescence and photoconductivity in $YBa_2Cu_3O_x$ show that oxygen vacancy defects (which act as F-centers) are central to the charge-transfer model. The correlation between the photoinduced conductivity and luminescence strongly suggests that the characteristic luminescence at 1.88 eV is indicative of the PPC/PISC state. The luminescence at 1.88 eV is a direct measure of the oxygen chain vacancy: As the number of oxygen vacancies decreases, the luminescence at 1.88 eV decreases. Moreover, photoluminescence studies imply that both the photogeneration and luminescent recombination of electron-hole pairs occur in the Cu-O chain layer.

As stated, further information concerning the energy levels and dynamics of the trapped electrons can be determined by optically probing the photoinduced state. In particular by illuminating a PISC/PPC sample with another pulse of light, one may potentially photoionize the F-centers thereby freeing the trapped electrons. Conceptually, one laser wavelength establishes PISC while another laser wavelength is used to quench (destroy) the photoinduced superconductivity state. The PISC state is

quenched as the freed electrons recombine with the photogenerated holes. Such an experiment serves two purposes: (1) The optimum laser wavelength for quenching is indicative of the energy depth of the traps and provides further evidence for the charge transfer-defect model of PISC/PPC. (2) The experiment demonstrates the possibility of an optically controlled superconducting circuit component; i.e., the photoinduced state could be initiated and quenched using two different pulses of light.

Numerous papers have suggested that the PISC phenomena has several practical applications such as optically controlled superconductive switches, microbridges, *in situ* laser fabrication and tuning of SC circuits [59], and storage and recording applications. One difficulty in using the PISC mechanism for optically controlled switching is that the photoinduced state is long-lived. In the case of laser-ablated $YBa_2Cu_3O_x$ films, the photoinduced state persists for days at 77^oK. While at low temperature no relaxation of the induced state occurs, slow relaxation of the photoconductivity towards the initial (pre-illumination) value does occur at room temperature. This relaxation time was described[17] as a thermally activated relaxation across on energy barrier of approximately 1 eV. In the oxygen vacancy defect model, the photoinduced state decays as trapped electrons are thermally released from the defect sites.

However, it has been established that the PISC/PPC state is reversible by heating the $YBa_2Cu_3O_x$ film. Gob et al. [60] have shown that it is possible to completely destroy the photoinduced state by exciting the electrons over this barrier merely be heating their samples to $320^oK$for 24 hours. The authors Gob et al. also surmise that since no PPC effect is detected in fully oxidized samples with suppressed T_c due to substitution of Yttrium atoms [22], the mechanism is related to the oxygen defects.

Their investigation focused on magnetoresistance (MR) measurements of an illuminated sample and an 'erased' sample. The authors observed a reduction in anisotropy of photoexcited, oxygen deficient $YBa_2Cu_3O_x$. However, under illumination, the increase in $\xi_{ab}(0)$ contrasts with the fact that $\xi_{ab}(0)$ for 90 Kelvin $YBa_2Cu_3O_x$is less that $\xi_{ab}(0)$ for T_c suppressed $YBa_2Cu_3O_x$. They arrive at the conclusion that there is more at work that the photogeneration of holes and assert that there may be decrease of defect density due to partial rearrangement of oxygen vacancies in the Cu-O chains. This effect may be larger that the photoinduced effect on $\xi_{ab}(0)$ thus producing the results observed. Overall, we note that the authors' results are consistent with the oxygen defect model. To date, only this thermal mechanism has been reported in the literature for erasing or quenching the photoinduced state. In this process, trapped electrons are thermally released from the defect sites and recombine with photogenerated holes. With a 1eV (as estimated by Kudinov et al. [17] energy barrier, long 'switching' times seem to be inherent to the PISC mechanism. (The thermal decay time scale is typically much longer (orders of magnitude) compared to the switching ON time.) The data shown is presented as evidence that this thermal decay constraint can be circumvented by using an *infrared laser (IR) beam to photoexcite trapped electrons thereby quenching the photoinduced superconductivity state on a time scale orders of magnitude faster than the thermal decay rate.*

6.2 Apparatus

In the second phase of this investigation process, we found that further information concerning the energy levels of the trapped electrons can be determined by illumi-

nating a PISC sample with another pulse of light which 'de-traps' the electrons. For this, the setup at the NJIT lab is quite similar to that of the initial photoluminescence studies. Films with oxygen contents of x=6.3 were chosen for this study. The photoinduced state is initiated with 4 W (all lines) of argon ion laser light. The photoinduced state is quenched using either 980 nm, 1300 nm, or 1480 nm lasers. The infrared laser spot sizes on the sample were adjusted to match that of the argon laser to ensure effective overlap. During illumination, the sample is immersed in liquid nitrogen to minimize the effect of sample heating.

6.3 Results

The photoinduced state is initiated by a 1 hour illumination with 4W (all lines) of argon ion laser light. During illumination, the sample is immersed in liquid nitrogen to minimize the effect of sample heating. Films with oxygen content of $YBa_2Cu_3O_{6.3}$ were chosen for study. Both before and after visible illumination, the resistance versus temperature curves of these films (not shown) show a negative slope at 77K. A purely thermally induced change in the resistance would result in a descrease in the measured resistivity at this ambient temperature. Upon illumination with the visible argon laser light, the measured resistance decreases by roughly 47% as shown in Figure 6.1. As shown in the inset, when the laser beam is blocked, the resistance maintains a constant value indicating negligable thermal induced changes.

The photoinduced state is quenched using either 980nm, 1300nm, or 1480nm lasers. The infrared laser spot sizes (~4mm) on the sample were adjusted to match that of the argon laser. Illumination of the photoinduced sample (*ie.* Time > 3600s of Figure 6.1)

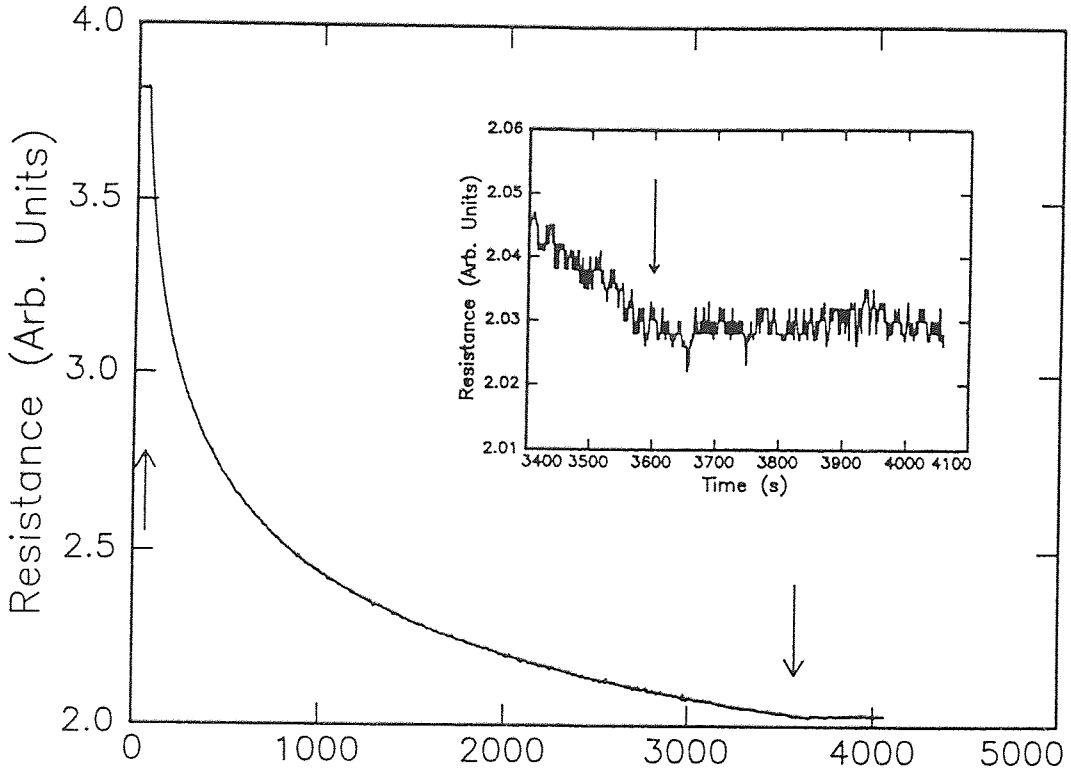

Figure 6.1 : Resistivity after illumination with Argon Ion light

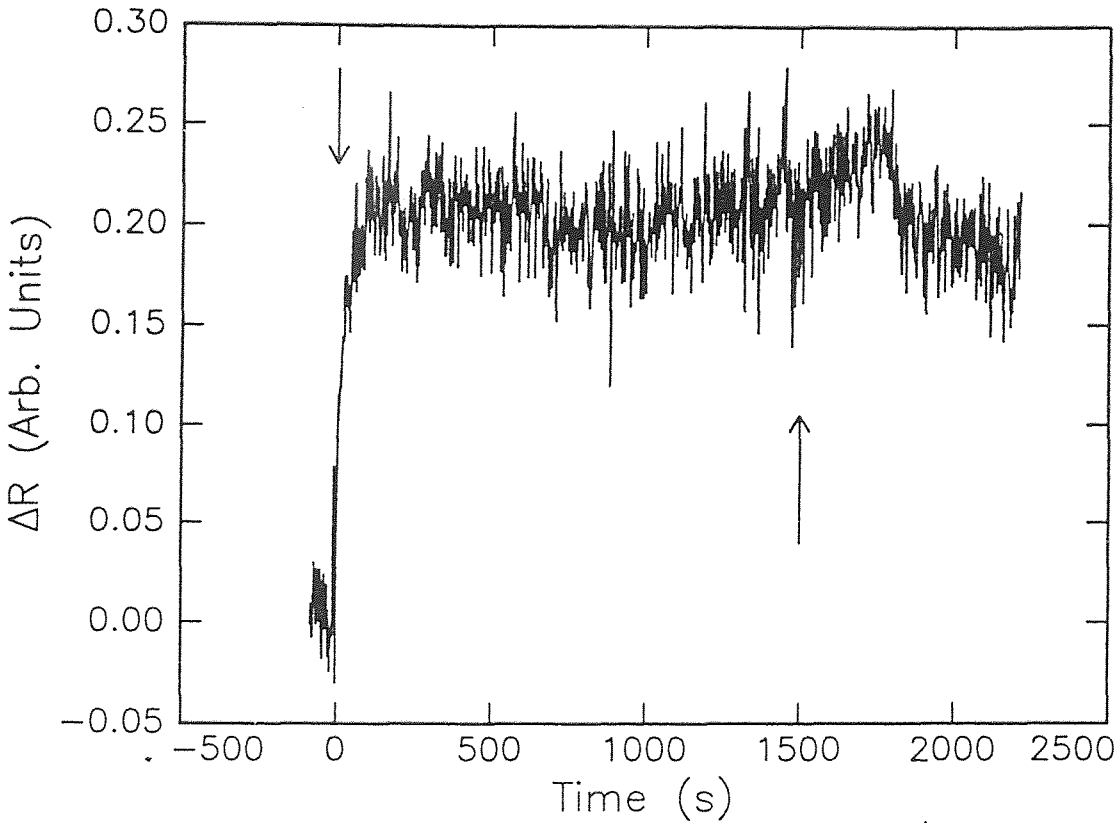

Figure 6.2 : Quenching IR light at 1300 nm

with low intensity infrared light increases the resistance as shown in Figure 6.2 (75 mW, 1300 nm) and 6.3 (90 mw, 1480 nm). The maximum change in resistance ΔR shown in Figure 6.2 corresponds to about 1.1% of the resistance drop induced by the 4 W illumination. The ΔR shown in Figure 6.3 represents 2.2% of the resistance drop induced in that film. The quenching process is reversible: After infrared quenching, illumination with argon light causes the sample resistance to decrease (not shown).

The IR intensity dependence is determined by attenuating the laser beams using neutral density filters. After quenching at a particular laser power, the photoinduced state is reestablished by a fifteen minute exposure to the 4W laser light. Figures 6.4 and 6.5 shows the intensity dependence of the change in resistivity ΔR subsequent

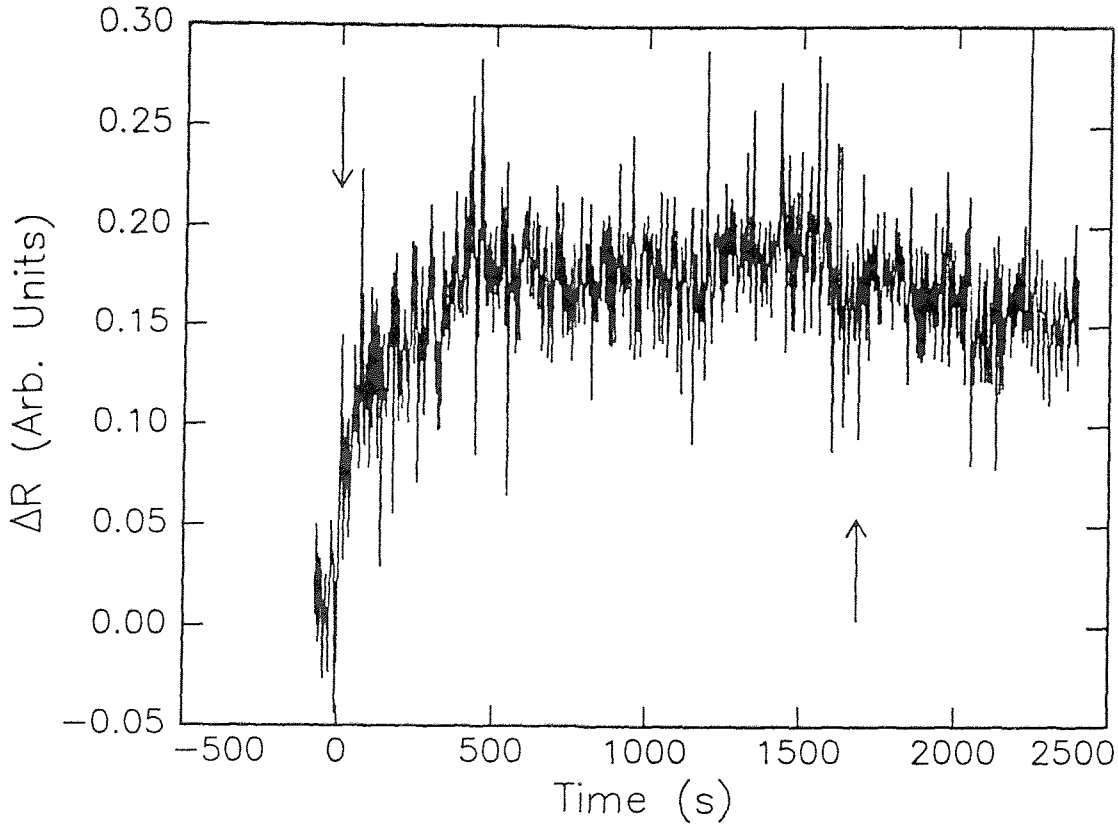

Figure 6.3 : Quenching IR light at 1480 nm

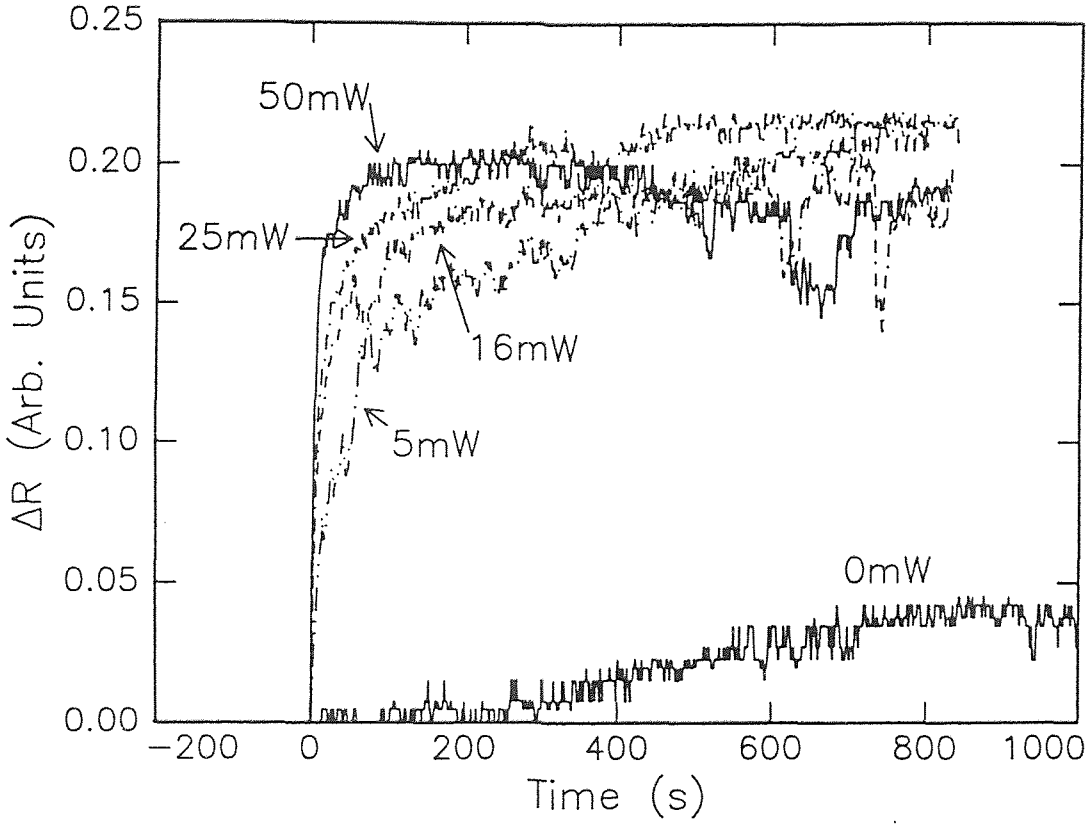

Figure 6.4 : Intensity dependence in quenching at 980 nm

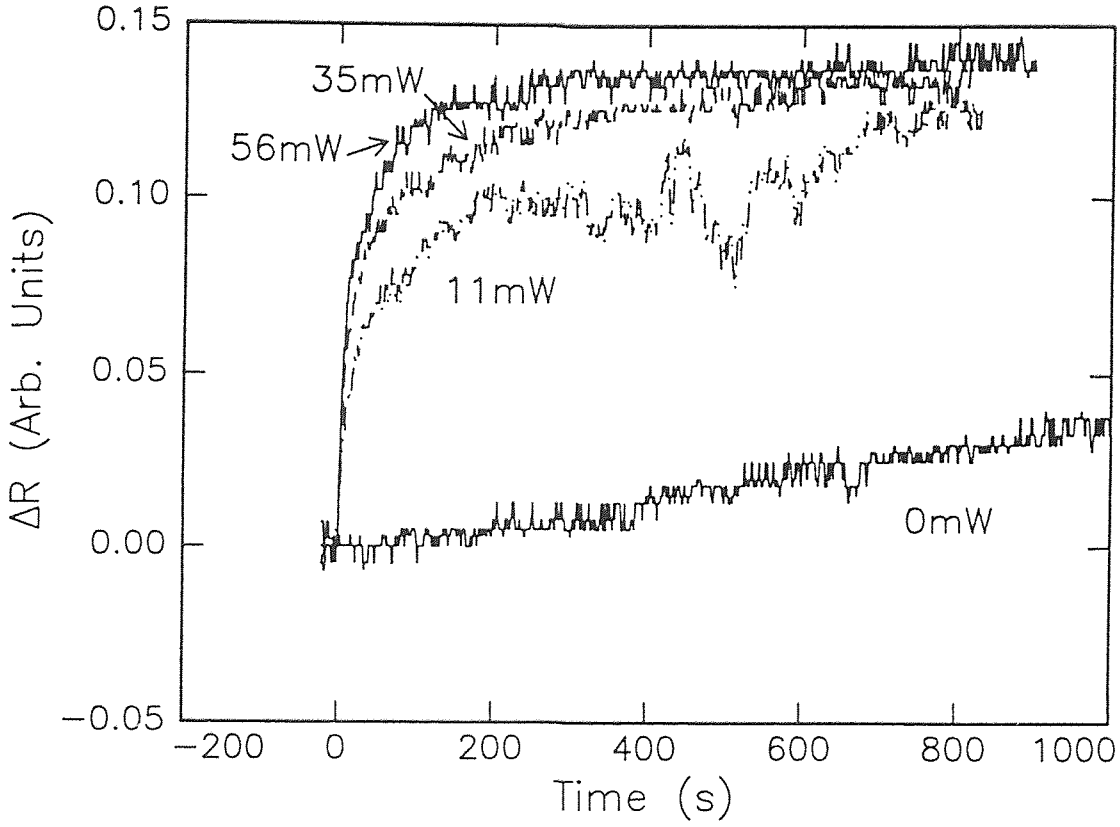

Figure 6.5 : Intensity dependence in quenching at 1480 nm

to illumination with infrared light at 980 nm (1.26 eV) and 1480 nm (.84 eV). These photon energies were chosen because they are close to the 1eV energy barrier inferred from thermal decay measurements.[17] For the sample data presented in Figure 6.4, 980nm light is approximately 1.5 times more efficient than 1480nm light in quenching the photoinduced state. For another sample, (Figure6.5) quenching via 1300nm light is 1.2 times more efficient than 1480nm light. Attempts to quench the PISC state using 800nm (1.55eV) light resulted in a further *decrease* in resistance. This result is consistent with the small PPC response reported previously[17, 20] at 800nm. The largest quenching (10%) was observed for 0.1W broadbanded infrared light (1-5μm).

6.4 Discussion

The IR quenching results can not be explained by simple sample heating:

- The photoinduced state is quenched (resistance increases upon illumination with infrared light) for samples in which the slope of their resistance versus temperature curve in the photoinduced state is negative. If the IR light were heating the film, the observed resistance would decrease rather than increase upon IR illumination. An increase in resistance with IR illumination is observed.

- As shown in Figure 6.1 and Figure 6.3, removing the potential heating source (blocking laser beam) does not lead to a change in the resistance.

- The data of Figure6.5 and Figure6.4 can not be fit using the thermal decay model of Reference [17]. In this model, the decay of the photoinduced conductivity as

a function of time can be described using a stretched exponential function

$$\Delta\sigma(t) = \sigma_o \exp(-(t/\tau)^{\beta}) \tag{6.1}$$

where the decrease in relaxation time with increasing temperature is described by thermally activated relaxation across an energy barrier:

$$\tau(T) = \tau_o \exp(\Delta/kT) \tag{6.2}$$

where $\Delta\sigma(t)$ is the photoinduced deviation of conductivity from an equilibrium value σ_o, τ is a characteristic decay time, and β is a dispersion parameter $0 < \beta < 1$. From Reference [17], the experimentally determined energy barrier is $\Delta = 0.935eV$. Following the analysis of Reference [17], photoinduced conductivity curves derived from the experimental results of Figures 6.3 and 6.2 (not shown) can not be fit by the stretched exponential function assuming that the IR laser illumination heats the film temperature above the ambient 77K. As shown in the figures, the resistivity $(1/\sigma)$ changes rapidly in the first 100 seconds and then approaches a constant value for long times. According to Equation (6.1), the photoinduced conductivity vanishes for long times.

- By comparing the results of 980, 1300, and 1480 nm illumination, the maximum change in resistivity depends on the IR wavelength and not the total power.

- Lastly, as the power of the infrared light is increased from 0 to >50 mW, the maximum change in resistivity seems to saturate. If the results were due to sample heating, the maximum change in resistivity should continue to increase as the infrared power is increased.

The data suggest that trapped electrons are photoexcited from the defect sites. As the IR power is increased, the rate of resistance change increases. This is consistent with a larger number of photons per second ionizing the trapped electrons. The time scale for quenching varies from roughly 60 s (980 nm) to 200 s (1480 nm) for Figure 6.4. For another film (Figure 6.5), quenching occurs in 100 and 500 s for 1300 and 1480 nm respectfully. In comparing the maximum change in resistance ΔR per photon for the different wavelengths, we calculate relative values of 15.4 (1.1% ΔR, 75 mW, 0.954 eV photon) and 12.2 (0.92% ΔR, 90 mW) for 1300 and 1480 nm respectfully in Figure 6.4. For Figure 6.5, the values are 34.6 (2.2% ΔR, 50mW) and 32 (1.5% ΔR, 56mW) for 980 and 1480nm respectfully. The wavelength dependence of the time scale and maximum ΔR suggests that the optimum wavelength and characteristic energy depth of the traps is about 0.95-1.26eV corresponding to 980-1300nm. This experimental value is consistent with the thermal activation energy of 1.0 eV.[17] While the thermal decay measurements of Reference [17] average over a distribution of energy levels, probing with a single wavelength allows one to distinguish among traps with different energy depths.

The saturation of ΔR with infrared power suggests two possible explanations: There is a distribution of defects with different energy levels ϵ where the width of the levels $\Delta\epsilon/\epsilon << 1$ is small. If the energy width were small, probing the defect energy levels near 1.26 eV (980 nm), for example, would not effect electrons trapped in defects with characteristic energy depths of 0.94 eV (1300 nm) or 0.83 eV (1480 nm). Electrons would remain trapped in those levels upon illumination with 1.26 eV light and consequently the quenched resistivity will not fully recover to its unilluminated

value. There are several mechanisms which could generate a distribution in defect energies. For example, the distribution of any Cu-O chain fragments near a particular defect would perturb the local potential. Likewise, grain boundaries may introduce a distribution of energy levels for defects Recent work of Moeckly *et. al*[61] highlights the role of chain site oxygen disorder driven by the elastic strain gradient near the grain boundary. Strain is introduced since the lattice structure is locally distorted at the boundaries. It may be possible that the strain gradient also perturbs the local potential thus creating a variation in defect energies throughout the sample. We are currently conducting IR quenching experiments with broadbanded light to test these scenarios.

Another interpretation of the ΔR saturation is that some defects may not be optically accessible i.e. they can not be photoionized. This scenario would explain why ΔR saturates and the quenched film resistance does not recover to its unilluminated value.

6.5 Summary

In conclusion, it has been shown that persistent photoconductivity is quenched in $YBa_2Cu_3O_x$ samples by excitation of electrons from the defect sites. The observed time scale for quenching is several orders of magnitude shorter than is achieved via thermal processes. The wavelength dependence of the IR quenching suggests that the average trap depth is $\sim$1 eV in agreement with previously published values inferred from thermal decay measurements. The maximum change in resistance ΔR is IR wavelength dependant and saturates above $\sim$50 mW. This suggests that either a

distribution of narrow energy band defect levels exist in $YBa_2Cu_3O_x$ or that some defects are not optically accessible for IR quenching.

CHAPTER 7

PROJECT FUTURE

7.1 Hall Measurements

For the third phase of this investigation, we attempt to observe changes in the Hall coefficient upon sample illumination. From these measurements it will be apparent that in the photoinduced state, the carrier density and mobility of the carriers are affected. A previous study [18] has shown that these quantities are indeed influenced by illumination on oxygen deficient $YBa_2Cu_3O_x$ samples. The authors Nieva et al. report that for a suppressed T_c sample of x= 6.5 they observed changes in resistivity ρ, mobility μ and hall coefficient R_H on the orders of -26%, -20%, and +20% respectively. The observed increase in carrier concentration is compliant with a photogeneration of holes that are then held separate from their electrons and not allowed to recombine.

Correlation of hall data to our electrical and photoluminescence data is important for the following reasons:

- Correlation will authenticate initial photoluminescence measurement and conclusion concerning carrier density from Phase I of Chapter 5.

- Correlation will further support conclusion that effects seen with the secondary infrared illumination is not heating. We expect to see that carrier density decreases, indicating that the electrons are being released from their traps and allowed to annihilate holes.

- Correlation will give additional measurement of quenching efficiency in terms of

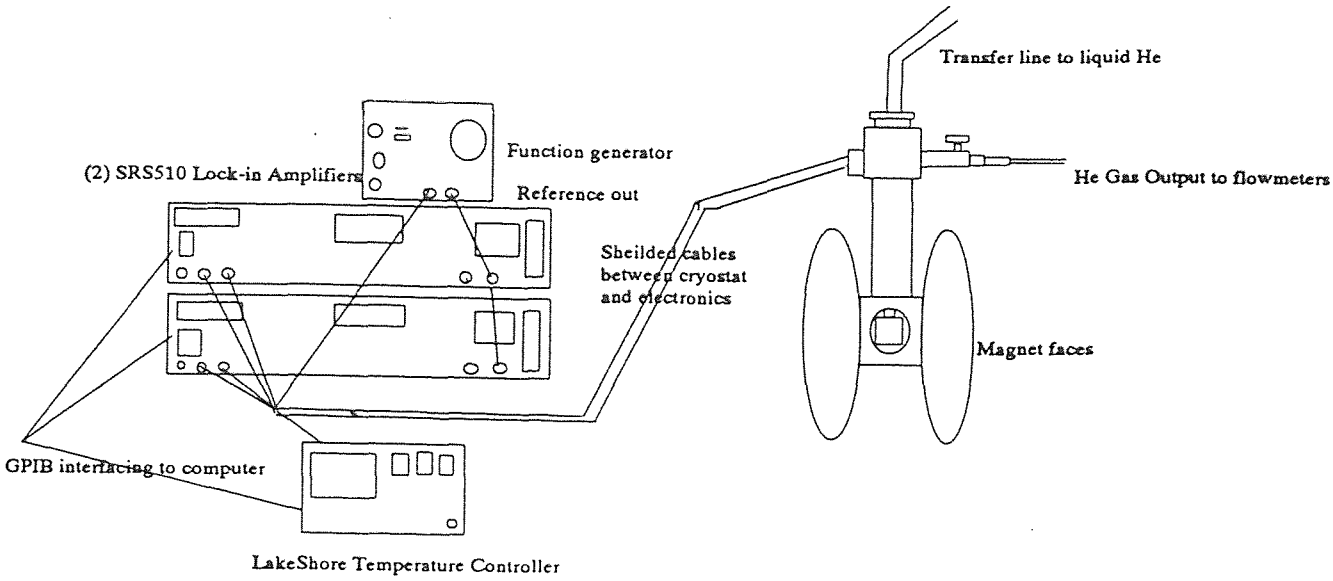

Figure 7.1 : Hall measurement set-up

carriers and defect levels which will further effectiveness of application efforts (to be discussed at later point).

For these measurements a patterned sample (Figure 4.5) of $YBa_2Cu_3O_x$ on $LaAlO_3$ is mounted with a thermally conducting/electrically insulating varnish on a copper block attached to a cold finger within sealed chamber under vacuum. Temperatures as low as $18°K$ may be achieved as desired when liquid helium is run through a transfer line to the coldfinger and through flow meters. A platinum diode varnished to the cold finger provides *in situ* information on chamber through a LakeShore temperature controller. Heater wire wrapped around the cold finger also allows for better temperature control. A desired temperature may be achieved by controlling the flow rate of the helium and the heater on the temperature controller.

The cryostat is mounted on a brace and is suspended in a water-cooled magnet

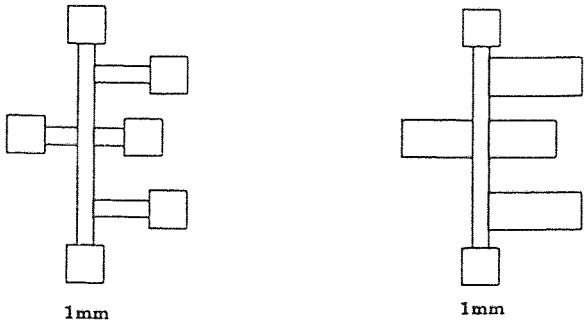

Figure 7.2 : New pattern for hall measurements

capable of producing a maximum field of 3000 Gauss. Current to the sample's primary channel is supplied by a function generator at a frequency of 100 Hz across a 500 Ω resistor to provide a current of the same order of magnitude as used by Nieva et al. [18]. Two Stanford Research System Series 510 lock-in amplifiers are triggered to the function generator and measure the resistance ρ and the Hall voltage V_H as seen in Figure 7.1. The entire data acquisition process is automated through a personal computer using GPIB interfacing and QBasic code originally provided by Savin of NJIT and modified by myself. The light source used for initial photoexcitation is a Xenon lamp. The light is focused and incident on the sample through a quartz window in the cryostat. Secondary illumination is performed with the same laser diodes as described in Chapter 6.

Initial problems of electromagnetic interference (EMI) were overcome by shielding all cables (RG-58 coax) and wires in braided cord or copper mesh. In this manner, the noise was reduced from orders of magnitude the same as the expected sample response (estimated to be on the order of μV) to two orders of magnitude less. Originally, it was also found that a constant offset of the Hall voltage occurred. Thermogravimetric effects and other [62, 12] possibilities such as temperature gradients across the sample

were eliminated as reasons for the constant voltage offest, leading us to believe that it may be caused by an physical offset of the leads attached to the sample. Thus a new patterning mask (Figure 7.2) in which the leads had a larger area (less chance of offset) was created. Use of this pattern for samples in subsequent measurements eliminated the previously observed offset.

Initial measurements show that heating effects are prevalent in the system. Work continues to better focus incoming light to sample to reduce substrate heating. The lag between sample temperature and the sensor (on cold finger and not directly attached to the sample) prevent reliable calculation of a correction factor to eliminate heating effects from Hall measurements. Minor refinements in optics arrangements are needed to accomplish this.

7.2 Surface Resistance Measurements

A collaboration with researchers at Notre Dame University is also underway to provide microwave surface resistance measurements of the $YBa_2Cu_3O_x$ materials. This effort is part of the Notre Dame group's larger scheme to substantiate the Blackstead-Dow [63] model which maintains that only *substitutional* oxygen vacancies in the Cu-O chain layers affect PISC and to devise a universal mechanism of superconductivity. The line of thought of the Blackstead-Dow model is in keeping with the oxygen defect model of F and F^+ centers trapping the electrons. A brief description of this work has been provided by group member Klunzinger, generalized, and included as part of this discussion. The ensuing sections describe $YBa_2Cu_4O_8$ their set-up and the preliminary results obtained.

7.2.1 Introduction: $YBa_2Cu_4O_8$& $YBa_2Cu_3O_x$ Systems

In the system of bulk $YBa_2Cu_4O_8$, it has been proposed that fluxon-antifluxon pair creation occurs due to the thermal fluctuations introduced by the laser light. In a two dimensional model for thin films described by Kadin et al.[64], fluxon-anitfluxon pairs remain bound at low temperatures and do not produce resistance, since they experience no net force from a current. At temperatures above the Kosterlitz-Thouliss [65] unbinding transition temperature (TKT), flux flow resistance occurs because the pairs are no longer bound, and Lorentz forces lead to a net core motion. For temperatures less than TKT, a large current can also lead to unbinding and an increase in resistance. Fischer [66] showed that a KT transition also occurs in three-dimensional layered superconductors. In the two dimensional picture, an incident photon creates a 'hotspot' that the transport current avoids. Essentially, $YBa_2Cu_4O_8$ bulk samples illuminated with laser light should produce higher resistance then when unillumi-nated. It is therefore expected that the induced increased resistance will relax to its unilluminated state rapidly after the laser light is turned off, since the supply of fluxon-antifluxon pairs also has been turned off [67]. The interaction of light and $YBa_2Cu_3O_x$ ($6 \leq x \leq 7 - \delta$) is as previously discussed in Chapter 4.

7.2.2 Experimental Equipment

The sample (either in thin film or bulk form) is placed in a standard liquid helium cryostat and a microwave spectrometer of novel design is used to monitor the surface resistance of the sample. One advantage of the microwave technique has over conventional point contact methods is that no electrical contacts are required. Thus,

the system is able to achieve very high current densities, on the order of 103 to 105 A/cm^2, without destructive dissipation in the contacts. In this case, the current is constrained to a small penetration depth, so the actual power dissipation is small. Contacts exposed to the radiation would also exhibit photoconductivity , injecting electrons into the sample.

The resonant cavity containing the sample is placed inside and inner chamber of the helium dewar which can be evacuated or filled with helium gas. A capillary tube connects the helium reservoir to the sample chamber, and the cooling rate is adjusted externally by using the capillary tube valve. The temperature is monitored using a GaAs diode sensor and controlled with a Lakeshore Model DRC 93C Temperaure Controller.

The microwave power is supplied by a klystron, and a microwave diode detects the power reflected from the cavity. At the resonant microwave frequency, the cavity exhibits minimum power reflections. The quality factor,Q, of the cavity is typically on the order of 103 for this system, and is related to the surface impedance of a superconductor which is $Z_s = R_s \times iX_s$: R_s is the surface resistance and X_s is the surface reactance. Changes in the surface resistance R_s with temperature and applied field lead to changes in the sample dissipation and the cavity Q, while changes in the surface reactance X_s lead to changes in the resonant frequency of the cavity. The Notre Dame system incorporates circuitry which "locks" the klystron source frequency to the cavity frequency: Consequently the variation in the reactance is not detected. Changes in power reflected from the cavity [68] are proportional to the incident power and changes in the effective resistance R_{c_e} of the sample bearing cavity.

The microwave diode detector mentioned above is used in conjunction with a directional coupler and responds to the power reflected by the cavity, which is proportional to the surface resistance. The cryostat is mounted in the gap of a Varian V-3900 Series Low Impedance magnet that can be varied from 1.6 Tesla; also available is a 7 Tesla superconducting magnet system, equipped with variable temperature capability. A 6 W Lexel 3500-SHG argon ion laser is used in the photoinduced conductivity experiments. The laser can be operated in a single line mode (typically 524.5 nm) or multi-line mode (all argon green wavelengths) . The laser beam is focused by a lens into a multimode 3M fiber optic cable with a core diameter of 200 μm. A separate fiber is routed from the wave guide through the center of the X-band wave guide. A SMA termination extends from the wave guide and is coupled to the laser injection fiber. The other end is polished and protrudes into the cavity. The fiber allows light to shine on the sample without itself having any effect on the microwave signal [67].

7.2.3 Preliminary Results

An oxygen deficient $YBa_2Cu_3O_x$ film we provided the Notre Dame group exhibited the expected PPC/PISC properties. Before illumination the film had a T_c of 39^oK. The film was illuminated at a temperature of $100^oK$with approximately 230 mW of multi-line green light from the argon ion laser for an hour. This corresponds to a value of 7.1×10^{21} photons/cm^2, as in the regime of Kudinov [17]. After illumination the film had a T_c of 43^oK. Also it was found that the T=0^oK intercept of the normal state resistance (measured in arbitrary units) had changed: $R/R_0 = .52$ a change that was reproduced reliably. Qualitative results with $YBa_2Cu_4O_8$ (not provided by our

group) samples indicate that the resistance increases as expected when illuminated with laser light. This occurred for illumination at temperature of $45°K$, $56°K$, and $100°K$. An immediate relaxation was seen when the laser light was turned off. The sample showed an increased signal when illuminated in a magnetic field of 1.6 Tesla at $75°K$ as well. Investigations into the possibility of heating effects are currently being performed.

7.2.4 Conclusion

The Notre Dame group also plans to extend the quenching experiments performed at NJIT to find the wavelength(s) of light that will efficiently turn 'off' the PPC/PISC effect. A Ti:Sapphire laser which is capable of producing wavelengths in the infrared region is being obtained. Both sets of experiments, the $YBa_2Cu_3O_x$ and the $YBa_2Cu_4O_8$ imply that there is a possibility of creating optically controlled switches from these materials. The $YBa_2Cu_4O_8$ however, is more stable and practical for devices because the oxygen does not leak in or out due to an extra Cu-O bond in the extra chain layer. On the other hand, films of this material are difficult to fabricate. In addition, the Notre Dame group envisions that the fundamental results of the $YBa_2Cu_4O_8$ experiments may contribute to the theories of fluxon-antifluxon pairs as well as provide evidence leading towards a universal theory of superconductivity.

7.3 Photoluminescence and Quenching Measurements

Other measurements in progress include photoluminescence spectra extension to search for further peaks at higher energies (above 2 eV). Also, samples spanning x=6 to x=7-

δ are to be fabricated . The effort also continues to probe the possible multiple defect levels by quenching at various wavelengths around the 1300 nm peak. The experiments outlined and discussed in Chapters 5 and 6 of this thesis work provide some insight into the previously proposed defect mechanism [15] while additionally indicating that the photogeneration and subsequent annihilation of the electron hole pairs occurs in the Cu-O chains rather than in the CuO_2 planes. However, each bit of new information obtained to answer a question in turns leads to yet other questions.

Photoluminescence

In this case, the photoluminescence spectra presented in Chapter 5 has been done for a limited range. Note that above 2 eV we have been unable to observe and peak changes due to illumination because of equipment limitations. The group has devised a means of overcoming this obstacle and hopes to report the results soon. The reported peaks in photoluminescence (Table 5.1) may have an response to illumination which may or may not be indicative of varying defect electronic structure. Efforts are also underway to test a spectrum of sample varying in oxygen content from x=6 to x=7-δ. We have presented data from samples in three specific regions of the oxygen content spectra; insulating, near the metal-insulator transition, and metallic.

Quenching

As discussed in Chapter 6, there may be structure within the general efficiency curve that we find to typify the quenching response of our films. This structure is hinted at by the saturation of the quenching effect for particular wavelengths. Note that

maximum change in resistance ΔR was found to be IR wavelength dependant. It was also observed to saturate above ~50 mW. This suggests that either a distribution of narrow energy band defect levels exist in $YBa_2Cu_3O_x$ or that some defects are not optically accessible for IR quenching. Probing this possibility by measuring the full IR spectra will enable us to determine which of these is true.

CHAPTER 8

FURTHER CONSIDERATIONS

8.1 Device Feasibility

As can be seen from the data presented in this thesis and in other works [14, 21], the excitation time of the induced states in thin films of $YBa_2Cu_3O_x$ is on the order of an hour or more. In today's technology, response times needed for applications are general much faster than offered by these thin films. It has long been noted that this effect may have application possibilities [69, 15, 17], but the reality that it is a long time scale effect has limited possible designs. For example, even to be able to incorporate optical switches in place where electro-mechanical switches currently exist, they would have to greatly improve. However, in single crystals of $YBa_2Cu_3O_x$ it has been observed that the excitation occurs in the temporal range of *pico to nano seconds* [13]. The primary and obvious difference between these two materials is the presence of grain boundaries in the thin films that are absent in the single crystal samples. Grain boundary effects on flux pining and critical current in $YBa_2Cu_3O_x$ and other high-T_c superconductors have been research subjects [70, 71, 72] over the past few years because of the restrictions they place on applications [69]. However, as of date, no research concerning grain boundary effects on the PPC/PISC phenomena or proposed mechanism has been presented. If this work were to be done, information concerning the manipulation of time scale effects would be valuable for application purposes. In addition to bringing the entire PPC/PISC effect within the range of use for current technology it may provide the capability to manufacture films with

specific response times for individualized purposes.

The fact that PISC exists in single crystal samples [13] indicates that the effect is inherent to the lattice properties themselves and not material properties such as the grain boundaries. It is generally believes that the region near the grain boundary is slightly oxygen deficient [69]. Hence, larger photoinduced effects can be expected for grain boundary junctions than for epitaxial thin films or single crystals. The time scales for excitation between the thin films and the single crystals differs greatly. Time scales for extinction/quenching processes have not investigated.

Tanabe et al.[69] find that the results of their current photoexcitation experiments with grain boundary junctions support the idea that there is a region with substantial oxygen deficiency and/or disorder and therefore a lower hole concentration near artificial grain boundaries in $YBa_2Cu_3O_x$. Data indicates that such a 'degraded' region contributes significantly to the resistance. The authors proceed to surmise that a photoinduced hole doping of oxygen deficient $YBa_2Cu_3O_x$ near the metal to insulator transition leads to a decrease in resistance, thus the observed reduction in resistance for grain boundary junctions can be explained by assuming a large contribution of the 'degraded' region to the resistance. Thus it would seen that due to a larger presence of defects in thin films versus single crystals, we will expect to see a greater PPC/PISC effect.

As of yet, we have been unable to find literature reporting the time dependence of PPC/PISC investigation in single crystals. The time dependence seems to be dependent on the efficiency of electron trapping by defects. Thus, the grain boundaries in thin films appear impede the process of 'trapping' which occurs so quickly in sin-

gle crystal sample samples. On the other hand, the reported effects of the trapping [18, 14] have not be investigated on a picosecond scale. It is possible that a picosecond response exists. It is also entirely possible that the trapping is efficient but that the detrapping (electron and hole recombination) is inhibited by the grain boundaries. The issue then becomes a matter of ascertaining grain boundary effects on the structure of the chains.

To investigate some of these effects, insulating films of x=6.1 and insulating single crystals of the same oxygen content should be examined. Since an effect of the grain boundary is to introduce greater oxygen defects in its locale, measurements comparing films and single crystal samples would provide information concerning the (non)dominance of the boundary effect. Recent work of Moeckly et al.[61] highlights the important role of the chain site oxygen disorder driven by the elastic strain gradient near the grain boundary. It may be possible that the strain gradient also affects the depths of the traps near the grain boundaries, thus creating a variation in well depths throughout the sample. An implication of this is that the electronic structure and possibly the lattice (on a small scale) is locally deformed at the grain boundary. In Chapter 6 (on Quenching) the possibility of multiple defect levels was discussed and supported by data showing that varying wavelengths provided different levels of quenching, indicating that not all trapped electrons are accessible to a particular energy. It would be worthwhile to investigate this by performing the same quenching experiments on single crystal samples. If all electrons were released upon illumination with the proper wavelength it would be evident that the defect energies are affected by the grain boundaries. If this does not turn out to be the case, it may imply that

there are multiple levels naturally occurring in the sample but will not rule out the possibility of a grain boundary mediated/dominated time scale response. Additional information concerning the role of grain boundaries can be found by examining the PPC/PISC and quenching properties of films as the grain size is controlled. Since other research areas have focused on grain boundary effects in $YBa_2Cu_3O_x$ for other electrical applications, the technology and methods for controlling grain sizes already exist. This knowledge will facilitate the production of samples for any future studies along these lines.

Overall, the demonstration of variations in photoluminescence intensity for illuminated $YBa_2Cu_3O_x$ and subsequent quenching of the effect supports and oxygen defect model. Based on this model, future research may be able to bring applications to fruition. Needless to say, such results will not revolutionize the electronics world as we know it, but will merely advance it while pushing forward the frontiers of science.

BIBLIOGRAPHY

[1] N. W. Ashcroft and N. D. Mermin. *Solid State Physics.* Saunders College Publishing, 1976.

[2] J. M. Ziman. *Principles of the Theory of Solids.* Cambridge University Press, 2 edition, 1972.

[3] C. Kittel. *Introduction to Solid State Physics.* John Wiley & Sons, 6 edition, 1986.

[4] A. C. Rose-Innes and E. H. Rhoderick. *Introduction to Superconductivity.* Pergamon Press, 1978.

[5] B, C, and S, *Phys. Rev. B* 1, (1956).

[6] C. C. Tsuei, A. Gupta, G. Trafas, and D. Mitzi, *Science* **263**, 1259, (1994).

[7] V. D. Shabetnik, S. Yu. Butuzov, and V. I. Platsii, *Pis'ma Zh. Tekh. Fiz.* **21**, 67, (1995).

[8] R. J. Cava, A. W. Hewat, E. A. Hewat, B. Batlogg, M. Marezioand, K. M. Rabe, J. J. Krajewski, W. F. Peck Jr., and L. W. Rupp Jr., *Physica C* **165**, 419, (1990).

[9] V. I. Kudinov, A. I. Kirilyuk, N. M. Kreines, R. Laiho, and E. Lahderanta, *Phys. Lett. A* **151**, 358, (1990).

[10] S. M. Trevor. *Photoconductivity in the Elements.* Academic Press, Inc.,Pub., 1952.

[11] R. H. Bube. *Photoconductivity of Solids.* John Wiley & Sons, 1960.

[12] E. H. Putley. *The Hall Effect and other related phenomena.* Butterworth & Co. Limited, 1960.

[13] G. Yu, C. H. Lee, A. J. Heeger, N. Herron, , E. M. McCarron, Lin Cong, G. C. Spalding, C. A. Nordman, and A. M. Goldman, *Phys. Rev. B* **45**, 4964, (1992).

[14] J. F. Federici, D. Chew, B. Welker, W. Savin, J. Gutierrez-Solana, T. Fink, and W. Wilber, *Physical Review B* **52**, 52, (1995).

[15] J. Hasen, D. Lederman, I. K. Schuller, V. Kudinov, M. Maenhoudt, and Y. Bruynseraede, *Physical Review B* **51**, 1342, (1995).

[16] V. I. Kudinov, I. L. Chaplygin, A. I. Kirilyuk, N. M. Kreines, R. Laiho, and E. Lahderanta, *Phys. Lett. A* **157**, 290, (1991).

[17] V. I. Kudinov, I. L. Chaplygin, A. I. Kirilyuk, N. M. Kreines, R. Laiho, E. Lahderanta, and C. Ayache, *Physical Review B* **47**, 9017, (1993).

[18] G. Nieva, E. Osquiguil, J. Guimpel, M. Maenhoudt, B. Wuyts, Y. Bruynseraede, M. B. Maple, and Ivan K. Schuller, *Appl. Phys. Lett.* **60**, 2159, (1992).

[19] J. F. Federici, B. I. Greene, D. R. Dykaar, F. Sharifi, and R. C. Dynes, *Phys. Rev. B* **46**, 11153, (1992).

[20] S. L. Bud'ko, H. H. Feng, M. F. Davis, J. C. Wolfe, and P. H. Hor, *Physical Review B* **48**, 16707, (1993).

[21] G. Nieva, E. Osquiguil, J. Guimpel, M. Maenhoudt, B. Wuyts, Y. Bruynseraede, M. B. Maple, and Ivan K. Schuller, *Phys. Rev. B* **46**, 14249, (1992).

[22] D. Lederman, J. Hasen, I. K. Schuller, E. Osquiguil, and Y. Bruynseraede, *Appl. Phys. Lett.* **64**, 652, (1994).

[23] C. Ayache, I. L. Chaplygin, A. I. Kirilyuk, N. M. Kreines, and V. I. Kudinov, *Sol. St. Comm.* **81**, 41, (1992).

[24] B. W. Veal, A. P. Paulikas, H. You, H. Shi, Y. Fang, and J. W. Downey, *Phys. Rev. B* **42**, 6305, (1990).

[25] B. W. Veal, H. You, A. P. Paulikas, Hao Shi, Y. Fang, and J. W. Downey, *Phys. Rev. B* **42**, 4770, (1990).

[26] V. J. Emery and S. A. Kivelson, *Physica C* **209**, 597, (1993).

[27] G. Yu, C. H. Lee, A. J. Heeger, N. Herron, , and E. M. McCarron, *Phys. Rev. Lett.* **67**, 2581, (1991).

[28] D. Mihailovic, C. M. Foster, K. F. Voss, T. Mertelj, I. Poberaj, and N. Herron, *Phys. Rev. B* **44**, 237, (1991).

[29] J. F. Federici, D. Chew, B. Welker, W. Savin, T. Fink, and W. Wilber, *Bull. Am. Phys. Soc.* **40**, 742, (1995).

[30] S. M. Sze. *Semiconductor Devices: Physics and Technology.* John Wiley & Sons, 1985.

[31] J. Cheung and J. Horwitz, *Material Research Society Bulletin* **XVII, No. 2**, 30, (1992).

[32] J. F. Ready, *Journal of Applied Physics* **36**, 462, (1965).

[33] M. Von Allmen, *Journal of Applied Physics* **47**, 5460, (1976).

[34] J. G. Andrews and D. R. Atthey, *J. Inst. Math. Appl.* **13**, 59, (1975).

[35] Y. V. Afana'ev and O. N. Krokhin, *Sov. Phys. JEPT* **25**, 639, (1967).

[36] S. I. Anisimov, *Sov. Phys. JEPT* **27**, 182, (1968).

[37] T. Venkatesan, X. D. Wu, A. Inam, and J. B. Wachman, *Appl. Phys. Lett.* **52**, (1988).

[38] D. J. C. Walker, A. Carrington, A. P. Mackenzie, and J. R. Cooper. Laser abaltion of $yba_2cu_3o_{7-x}$ thin films for fundamental physical studies.

[39] P.K. Gallagher, *Adv. Ceramic Material* **2**, 632, (1987).

[40] S. C. Tidrow. Private communication with the author.

[41] S. C. Tidrow, R. T. Lareau, A. Tauber, D. W. Eckart, W. D. Wilber, R. L. Pfeffer, and R. D. Finnegan. Oxygen processing of htsc materials and multilayer device structures. (Presentation at U.S Army Reseach Laboratory, Electronics and Power Sources Directorate, AMSRL-EP-EC-H, Fort Monmouth, NJ 07703-5601).

[42] E. Takayama-Muromachi, Y. Uchida, M. Ishii, T. Tanaka, and K. Kato, *Japanese Journal of Applied Physics* **26**, L1156, (1987).

[43] A. Ono, *Japanese Journal of Applied Physics* **26**, L1223, (1987).

[44] D. W. Cooke, M. S. Jahan, J. L. Smith, M. A. Maez, W. L. Hults, I. D. Raistrick, D. E. Peterson, J. A. O'Rourke, S. A Richardson, J. D. Doss, E. R. Gray, B. Rusnak, G. P. Lawrence, and C. Fortgang, *Applied Physics Letters* **54**, 960, (1989).

[45] D. W. Cooke, B. Bennett, E. R. Gray, R. J. Houlton, W. L Hults, M. A. Maez, A. Mayer, J. L. Smith, and M. S. Jahan, *Applied Physics Letters* **55**, 1038, (1989).

[46] D. W. Cooke, M. S. Jahan, E. R. Gray, J. L. Smith, W. L. Hults, and B. L. Bennett M. A. Maez, *J. Luminescence* **48**, 819, (1991).

[47] M. Roth, A. Halperin, and S. Katz, *Sol. St. Comm.* **67**, 105, (1988).

[48] Ch. B. Lushchik, I. L Kussmann, E. Kh. Fel'dbakh, P. Kh. Liblik, T. I. Savikhina, and I. A. Meriloo, *Sov. Phys. Solid State* **29**, 2097, (1987).

[49] Ch. B. Lushchik, I. L Kussmann, E. Kh. Fel'dbakh, K. E. Vallaste, P. Kh. Liblik, A. A. Maaroos, I. A. Meriloo, and T. I. Savikhina, *JETP Lett.* **46**, 151, (1987).

[50] I. Ya Fugol, V. N. Samovarov, Yu. I. Rybalko, and V. M. Zhuravlev, *Sov. J. Low Temp. Phys.* **16**, 337, (1990).

[51] V. G. Stankevich, N. Yu. Svechnikov, K. V. Kaznacheev, R. A Kink, I. L. Kuusmann, E. Kh. Feldbach, G. Zimmerer, T. Kloiber, A. A. Zhokhov, G. A Emel'chenko, M. A. Kalyagin, and V. Ya Kosyev, *J. Luminescence* **48**, 845, (1991).

[52] V. G. Stankevich, N. Yu. Svechnikov, K. V. Kaznacheev, R. A Kink, I. L. Kuusmann, E. Kh. Feldbach, G. Zimmerer, T. Kloiber, A. A. Zhokhov, G. A Emel'chenko, M. A. Kalyagin, and V. Ya Kosyev, *Nucl. Instr. Meth. Phys. Res. A* **308**, 8193, (1991).

[53] M. N. Popova, A. V. Puyats, M. E. Springis, and E. P. Khlybov, *JETP Lett.* **48**, 667, (1988).

[54] V. V. Eremenko, I. Ya. Fugol', V. N. Samovarov, and V. M. Zhuravlev, *JETP Lett.* **47**, 619, (1988).

[55] V. N. Andreev, B. P. Zakharchenya, S. E. Nikitin, F. A. Chudnovskii, E. B. Shadrin, and E. M. Sher, *JETP Lett.* **46**, 492, (1987).

[56] B. J. Luff, P. D. Townsend, and J. Osbourne, *J. Phys. D: Appl. Phys.* **21**, 663, (1988).

[57] D. W. Cooke, H. Rempp, Z. Fisk, J. L. Smith, and M. S. Jahan, *Physical Review B* **36**, 2287, (1987).

[58] S. L. Cooper, D. Reznik, A. Kotz, M. A. Karlow, R. Lui, M. V. Klein, W. C. Lee, J. Giapintzakis, D. M. Ginsberg, B. W. Veal, and A. P. Paulikas, *Physical Review B* **47**, 8233, (1993).

[59] K. Tanabe, S. Kubo, F. Teherani, H. Asano, and M. Suzuki, *Jap. J. Appl. Phys. L* **32**, 264, (1993).

[60] W. Gob, W. Lang, W. Markowitsch, V. Schosser, W. Kula, , and Roman Sobolewski, *Sol. St. Comm.* **96**, 431, (1995).

[61] B. H. Meockly, D. K. Lathrop, and R. A. Buhrman, *Phys. Rev. B* **47**, (1993).

[62] Proceedings fo the I.R.E. *Hall Effect*, 1952.

[63] H. A. Blackstead and J. D. Dow, *JEPT Lett.* **59**, 283, (1994).

[64] A. M. Kadin, M. Leung, A. D. Smith, and J. M. Murdock, *Physica B* **169**, 681, (1991).

[65] M. Tinkham. *Introduction to Superconductivity.* McGraw Hill, 1975.

[66] K. H. Fischer, *Physica C* **178**, 191, (1991).

[67] A. Klunzinger. Information concerning the principles of their current investigation and the specifics of the experiemtal equipment and preliminary results have been provided by the Notre Dame group.

[68] G. Feher, *Bell System Tech J.* **36**, 449, (1957).

[69] K. Tanabe, F. H. Teherani, S. Kubo, H. Asano, and M. Suzuki, *Journal of Applied Physics* **76**, 3679, (1994).

[70] M. Arvano, K. Kani, Y. Takao, and H. Takagi, *J. of Cer. Soc. of Japan* **100**, 434, (1992).

[71] R. L. Meng, L. Gao, P. Gautier-Picard, D. Ramirez, Y. Y. Sun, and C. W. Chu, *Physica C* **232**, 337, (1994).

[72] Y. Tomkiya, T. Tanaka, X. Zheng, H. Kuriyaka, and K. Hirakawa, *Physica C* **219**, 288, (1994).